Title

A radiation closure study of Arctic stratus cloud microphysical properties using the collocated satellite-surface data and Fu-Liou radiative transfer model

Journal

Journal of Geophysical Research: Atmospheres, 121(17)

ISSN

2169-897X

Authors

Dong, Xiquan
Xi, Baike
Qiu, Shaoyue
et al.

Publication Date

2016-09-16

DOI

10.1002/2016jd025255

Peer reviewed

A radiation closure study of Arctic stratus cloud microphysical properties using the collocated satellite-surface data and Fu-Liou radiative transfer model

Xiquan Dong[1], Baike Xi[1], Shaoyue Qiu[1], Patrick Minnis[2], Sunny Sun-Mack[3], and Fred Rose[3]

[1] Department of Atmospheric Sciences, University of North Dakota, Grand Forks, North Dakota, USA, [2] NASA Langley Research Center, Hampton, Virginia, USA, [3] SSAI, Inc., Hampton, Virginia, USA

Correspondence to: X. Dong, dong@aero.und.edu

Abstract

Retrievals of cloud microphysical properties based on passive satellite imagery are especially difficult over snow-covered surfaces because of the bright and cold surface. To help quantify their uncertainties, single-layered overcast liquid-phase Arctic stratus cloud microphysical properties retrieved by using the Clouds and the Earth's Radiant Energy System Edition 2 and Edition 4 (CERES Ed2 and Ed4) algorithms are compared with ground-based retrievals at the Atmospheric Radiation Measurement North Slope of Alaska (ARM NSA) site at Barrow, AK, during the period from March 2000 to December 2006. A total of 206 and 140 snow-free cases ($R_{sfc} \leq 0.3$), and 108 and 106 snow cases ($R_{sfc} > 0.3$), respectively, were selected from Terra and Aqua satellite passes over the ARM NSA site. The CERES Ed4 and Ed2 optical depth (τ) and liquid water path (LWP) retrievals from both Terra and Aqua are almost identical and have excellent agreement with ARM retrievals under snow-free and snow conditions. In order to reach a radiation closure study for both the surface and top of atmosphere (TOA) radiation budgets, the ARM precision spectral pyranometer-measured surface albedos were adjusted (63.6% and 80% of the ARM surface albedos for snow-free and snow cases, respectively) to account for the water and land components of the domain of 30 km × 30 km. Most of the radiative transfer model calculated $SW^{\downarrow}_{sfc}$ and $SW^{\uparrow}_{TOA}$ fluxes by using ARM and CERES cloud retrievals and the domain mean albedos as input agree with the ARM and CERES flux observations within 10 W m^{-2} for both snow-free and snow conditions. Sensitivity studies show that the ARM LWP and r_e retrievals are less dependent on solar zenith angle (SZA), but all retrieved optical depths increase with SZA.

1 Introduction

Cloud macrophysical and microphysical properties have a significant impact on the radiative energy budgets at both the surface and top of atmosphere (TOA). The cloud-radiative interactions in the Arctic are even more complex due to large solar zenith angles, highly reflective snow and ice surfaces, and multiple reflections of solar radiation between the cloud layer and highly reflective snow/ice surfaces [*Curry et al*., 1996; *Dong et al*., 2010]. Minimal visual and thermal contrasts exist between Arctic clouds and the snow- and

ice-covered surfaces beneath them, which can lead to difficulties in passive satellite retrievals of cloud properties. This is especially true when visible and infrared wavelengths are used [*Spangenberg et al*., 2004; *Curry et al*., 1996]. Numerous studies of cloud-radiation interactions have been performed in this area, including the First International Satellite Cloud Climatology Project Regional Experiment (FIRE) Arctic Cloud Experiment (ACE) [*Curry et al*., 2000], the Surface Heat Budget of the Arctic Ocean project [*Uttal et al*., 2002], and the Mixed-Phase Arctic Cloud Experiment [*Verlinde et al*., 2007]. However, many questions remain concerning our understanding of the physical and dynamical processes of Arctic clouds and the retrievals of cloud properties over snow surfaces using passive satellite imagery.

The NASA Clouds and Earth's Radiant Energy System (CERES) project was created to aid the understanding of global cloud-radiative interactions by simultaneously measuring cloud properties and radiation fields at the TOA by using instruments onboard the Terra and Aqua satellites [*Wielicki et al*., 1998]. *Minnis et al.* [2011a] developed a set of algorithms for CERES Edition 2 (Ed2) to derive cloud macrophysical and microphysical properties (water droplet effective radius r_e, optical depth τ, and liquid water path (*LWP*)) for each Moderate Resolution Imaging Spectroradiometer (MODIS) pixel within a CERES Single Scanner Footprint (SSF) that was classified as cloudy by the CERES cloud mask [*Minnis et al*., 2008]. The CERES Ed2 low-level cloud retrievals over land have been compared with the Department of Energy (DOE) Atmospheric Radiation Measurement (ARM) [*Ackerman and Stokes*, 2003] Southern Great Plains (36.6°N, 97.5°W) observations and retrievals [*Dong et al*., 2008], but to date have not been evaluated over snow-covered surfaces.

The CERES Ed2 cloud products are used in the CERES Edition 3 (Ed3) energy balance product [*Loeb et al*., 2009] and a suite of other parameters generated for CERES Ed2 and Ed3. They will continue to be produced through 2016. A revised set of cloud algorithms has been developed to accompany a variety of other updates to the CERES analysis systems that are designated CERES Edition 4 (Ed4) [see *Minnis et al.*, 2010a]. The Ed4 algorithms are being applied to all of the measurements taken by CERES on the Terra and Aqua satellites from launch into the future past 2016. The CERES Ed4 retrievals of marine boundary layer overcast cloud properties have been compared with the retrievals of similar quantities by using measurements taken at the DOE ARM Mobile Facility Azores site [*Xi et al*., 2014], but similar evaluations have not been performed for clouds over snow. One of the main changes in the cloud algorithms has been the use of the MODIS 1.24 μm channel to retrieve cloud optical depth τ over snow and ice surfaces for Ed4 instead of either the 1.6 or 2.1 μm channel used for Ed2. The mean Ed4 retrievals of τ over polar regions are by 25–100% greater than their Ed2 counterparts [*NASA*, 2016]. Without statistically meaningful validations over high-latitude areas, it is not clear which channel yields the

most accurate retrievals. In either case, it is important to know how each of the algorithms performs in polar conditions.

The DOE ARM North Slope of Alaska (NSA; 71.3°N, 156.6°W) site at Barrow, AK, has been operating a variety of instruments since 1997. The site is situated on tundra within 2 km of the coast and surrounded by several large ponds and a lagoon. It and the adjacent waters are covered by snow/ice from late September to early June [*Dong et al*., 2010]. Furthermore, the site could be snow-free while ice could remain in the water or vice versa. Thus, the background can be very heterogeneous when viewed from a satellite as will be discussed in section 2.4. The instruments at the site include cloud radars, various radiometers, and radiosondes that can be used to estimate a variety of cloud parameters useful for studying cloud processes and comparing with satellite retrievals. To begin the process of validating the Ed2 and Ed4 retrievals at high latitudes and over snow-covered surfaces, this study compares single-layered overcast stratus cloud properties determined from the ARM NSA measurements with matched Ed2 and Ed4 retrievals from Terra and Aqua.

The comparisons use data taken from March 2000 to December 2006. During the 7 year period, a total of 206 and 140 snow-free cases (broadband surface albedo, $R_{sfc} \leq 0.3$) from Terra and Aqua satellites, respectively, have been selected for comparing the CERES Ed2 and Ed4 retrieved cloud microphysical properties with the ARM retrievals. For snow cases ($R_{sfc} > 0.3$), there are a total of 108 Terra cases and 106 Aqua cases, respectively. As a means to further validate these cloud retrievals, these cloud properties (both ARM and CERES retrieved cloud-droplet effective radius r_e and τ, as well as ARM-measured cloud base and cloud top heights and R_{sfc}), the estimated domain mean albedos are used as input for the NASA Langley modified Fu-Liou radiative transfer model (RTM) to calculate the downward shortwave ($SW^{\downarrow}_{sfc}$) flux (and transmission, γ) at the surface and reflected SW ($SW^{\uparrow}_{TOA}$) flux (and albedo, R_{TOA}) at the TOA. These calculations are then compared with the collocated ARM surface and CERES TOA radiation observations to determine how well they provide radiation closure. Through this study, we seek to tentatively answer the following three scientific questions:

To what degree do the CERES Ed2 and Ed4 cloud microphysical properties agree with the ARM retrievals over snow-free and snow surfaces?

To what percentages do the RTM calculated downward SW flux and transmission at the surface and reflected SW flux and albedo at the TOA agree with the collocated ARM surface and CERES TOA observations?

How sensitive the retrieved cloud properties, as well as observed and RTM-calculated radiative fluxes, vary with solar zenith angle (*SZA*) and surface albedo (R_{sfc}) under snow-free and snow conditions?

2 Data and Methods

The ARM ground-based observations and retrievals were averaged over a 1 h interval centered at the time of each satellite overpass, and the CERES Ed4 and Ed2 cloud and radiation properties were averaged within a 30 km × 30 km box centered on the ARM NSA site. Note that for low-level winds of 10 m s^{-1}, the 1 h averaging interval used in this study is equivalent to a frozen turbulence spatial scale of 36 km. In a statistical context, the temporally averaged surface observations should be equivalent to the spatially averaged satellite results, as demonstrated by *Dong et al.* [2008]. A sensitivity study has been performed on the grid box size (100 km × 100 km versus 30 km × 30 km), and the results show that the box size will not significantly influence the satellite cloud retrievals and TOA fluxes. Note that this sensitivity study is for the overcast and low-level stratus cloudy cases, whereas the conclusion may not be valid for clear-sky conditions due to different albedos of land and ocean. In this study, only single-layered overcast liquid-phase and liquid dominant mixed-phase Arctic stratus clouds are studied here because they are simplest cloud type to interpret from both the surface and the satellites.

2.1 Ground-based Measurements and Retrievals

The millimeter wavelength cloud radar (MMCR) [*Moran et al*., 1998] is a vertically pointing radar that operates at a wavelength of 8.6 mm and provides radar reflectivity profiles of hydrometeors moving through the radar field of view. This allows for the identification of both cloudy and clear conditions at the ARM NSA site. The MMCR is sensitive to the sixth moment of the cloud particle distribution, while the micropulse lidar (MPL) and laser ceilometer are sensitive to the second moment. Consequently, many studies have combined radar and lidar measurements to estimate cloud fraction and boundaries [e.g., *Intrieri et al*., 2002; *Dong et al*., 2005, 2010]. In this study, the single-layered overcast stratus clouds were selected by the ARM radar-lidar observations, then verified by the CERES cloud retrievals, and finally classified into the following two categories: snow-free ($R_{sfc} \leq 0.3$) and snow ($R_{sfc} > 0.3$).

Cloud top height is derived from the ARM MMCR reflectivity measurement, and cloud base height is derived from a combination of MMCR, MPL, and laser ceilometer data as described by *Clothiaux et al.* [2000]. The cloud liquid water path (*LWP*) is derived from microwave radiometer brightness temperatures at 23.8 and 31.4 GHz by using the statistical retrieval method described by *Liljegren et al.* [2001] with uncertainties of ~20 g m^{-2} for *LWP* below 200 g m^{-2} and 10% for *LWP* exceeding 200 g m^{-2} [*Dong et al*., 2000; *Liljegren et al*., 2001]. The upward and downward looking standard Eppley precision spectral pyranometers (PSPs) provide measurements of hemispheric downward and upward broadband shortwave (SW, 0.3–3 μm) fluxes at the surface, respectively, and quality checked by using the QC radiation value added product [*Long and Shi*, 2008]. Estimates of uncertainties for global SW (measured by unshaded PSPs) and total SW-down (the sum of direct and diffuse SW-down fluxes) fluxes are 10 W m^{-2} [*Long*

and Shi, 2008]. The global SW fluxes have been corrected for IR loss by using the method of *Younkin and Long* [2003]. Broadband R_{sfc} is derived from the ratio of $SW^{\uparrow}_{sfc}$ to $SW^{\downarrow}_{sfc}$ flux measurements, and γ is calculated from the ratio of cloudy $SW^{\downarrow}_{sfc}$ flux to clear-sky $SW^{\downarrow}_{sfc}$ flux that was estimated by the empirical curve-fitting technique of *Long and Ackerman* [2000].

To retrieve the daytime microphysical properties of single-layered overcast stratus clouds, the approaches taken by *Dong et al*. [1997, 1998] were used, with a modification to include surface albedo introduced by *Dong and Mace* [2003]. During the retrieval process, a δ2-stream radiative transfer model was used with the input of ground-based measurements in order to retrieve the layer-mean microphysical properties of single-layered overcast stratus clouds. *Dong and Mace* [2003] developed a new parameterization of cloud properties based on the retrieved cloud microphysical properties from a total of 13 single-layered overcast stratus clouds (~91 h of data) with a range of R_{sfc} from 0.1 to 0.8. The retrieved values of layer-mean cloud-droplet effective radius (r_e) from the *Dong and Mace* [2003] methods were parameterized as a polynomial function of *LWP*, γ, cosine of SZA (μ_0), and R_{sfc} as follows:

$$r_e = 2.49\mathrm{LWP} + 10.25\left(1 - R_{sfc}^3\right)\gamma - 0.25\mu_0 + 20.28\mathrm{LWP}\gamma\left(1 - R_{sfc}^3\right) - 3.14\mathrm{LWP}\mu_0, \quad (1a)$$

where the units of *LWP* and r_e are (100 g m^{-2}) and (μm), respectively. Once r_e is known, τ can be estimated by the expression

$$\tau = \frac{3\mathrm{LWP}}{2r_e\rho_w}. \quad (1b)$$

Comparisons of the retrievals with the aircraft in situ measurements over the midlatitudes revealed that the uncertainties of the surface-retrieved r_e, τ, and *LWP* values under snow-free conditions are approximately 10% [*Dong et al*., 1998, 2002]. Over the snow/ice covered surfaces, the uncertainties of the surface retrievals are nearly double those for retrievals over snow-free conditions based on the aircraft in situ measurements during FIRE-ACE in May 1998 [*Dong et al*., 2001] and to other aircraft in situ measurements near the ARM NSA site as discussed in section 4d of *Dong and Mace* [2003].

2.2 Satellite Observations and Retrievals

The CERES microphysical properties were computed from the CERES Single Scanner Footprint (SSF) product [*NASA*, 2014]. The SSF combines CERES (20-km@nadir) TOA broadband flux measurements with concurrent sampled 1 km cloud properties retrieved from MODIS along with a variety of other parameters including MODIS aerosol retrievals. Every fourth MODIS pixel along track on every other scan line is used in the CERES cloud analysis. For CERES Ed2, the MODIS pixels are classified as either cloudy or clear based on a cloud mask for polar regions [*Trepte et al*., 2002] that utilizes the 0.64, 1.62 (2.13), 3.78, 10.8, and 12.0 μm MODIS channels. The Ed4 polar mask had a number of updates including new tests that utilize the same suite channels along with the 1.38, 6.7, 8.5, and 13.3 μm channels. For this study,

the SSF values are averaged for all of the CERES footprints having a center within a 30 km × 30 km box centered on the ARM NSA site.

Several retrieval methods are used by CERES to derive Arctic cloud information from MODIS data. The CERES Ed2 retrieval methods for cloud microphysical properties have been described in detail by *Minnis et al.* [2011a, 2011b]. *Minnis et al.* [2010a] briefly described the algorithm changes for Ed4 processing. During daytime conditions (SZA < 82°) over snow-free surfaces, cloud microphysical and macrophysical properties are retrieved by using the four-channel visible-infrared shortwave-infrared split-window technique (VISST). The VISST employs the visible (0.63 μm), shortwave-infrared (3.7 μm), infrared (10.8 μm), and the split-window (12 μm) bands to estimate several cloud parameters, including r_e and τ. Because of high surface albedos at 0.63 μm channel for snow and ice-covered scenes, the shortwave-infrared infrared near-infrared technique (SINT) is used in these cases. The SINT takes advantage of the relatively small snow/ice albedos at some near-infrared wavelengths and is essentially the same as the VISST, except that for Ed2, the 1.6 μm (Terra) or 2.1 μm (Aqua) channel is used instead of the visible channel to estimate τ. The Aqua analyses used the 2.1 μm channel because its 1.6 μm channel was malfunctioning. The major changes from Ed2 to Ed4 that are relevant for this study include the following: calibration updates, bug fixes, an improved ozone absorption parameterization, new seasonal and regional boundary layer lapse rates for cloud height retrieval, and the use of 1.24 μm channel in the SINT instead of the 1.6 and 2.1 μm channels [*Minnis et al*., 2010a]. The clear-sky 0.63 and 1.24 μm albedos from *Chen et al.* [2006, 2010] were used to compute the background reflectances for the VISST and SINT cloud retrievals, respectively. Over snow-free surfaces within the domain, the clear-sky 0.63 μm albedo varies from 0.075 to 0.150 for solar zenith angle, SZA = 66°, while the 1.24 μm snow-covered clear-sky albedo ranged from 0.28 to 0.40 for the same SZA. The actual reflectance used for each retrieval varies with viewing and illumination angles and the dominant scene type within a given 32 km × 32 km CM analysis tile.

Su et al. [2015a] described the methodology used to develop the next-generation CERES angular distribution models (ADMs), which were developed by using the latest cloud algorithms [*Minnis et al*., 2010a]. These newly developed ADMs are used to produce the Ed4 SSF TOA/surface flux and cloud products for Terra and Aqua, whereas the fluxes in the Ed2 SSF products are inverted by using the ADMs described in *Loeb et al.* [2005, 2007]. The uncertainties of the Ed4 TOA instantaneous SW fluxes using the new ADMs have decreased significantly relative to Ed3, particularly at high latitudes [*Su et al*., 2015b]. For example, the clear-sky TOA instantaneous SW flux uncertainties are about 2.3% (1.9 W m^{-2}), 1.6% (4.5 W m^{-2}), and 2.0% (6.0 W m^{-2}) over ocean, land, and snow/ice surface, respectively. For all-sky conditions, the corresponding uncertainties are about 3.3% (9.0 W m^{-2}), 2.7%

(8.4 $W\,m^{-2}$), and 3.7% (9.9 $W\,m^{-2}$). TOA broadband albedo (R_{TOA}) is calculated as the ratio of $SW^{\uparrow}_{TOA}$ to $SW^{\downarrow}_{TOA}$.

2.3 Langley Modified Fu-Liou Radiative Transfer Model (RTM)

The NASA Langley modified Fu-Liou radiative transfer model (RTM) is a gamma-weighted two-stream approximation that uses inputs of linear and logarithmic averages of τ to account for cloud horizontal inhomogeneity [*Kato et al*., 2005]. The original Fu-Liou six broad SW bands have been expanded into 18 to improve the treatment of Rayleigh scattering, aerosols, and ozone, as well as to better understand the higher spectral resolution of ice absorption in 0.69–1.9 μm near-IR region [*Rose et al*., 2006]. In this study, $SW^{\downarrow}_{sfc}$ flux and γ at the surface and $SW^{\uparrow}_{TOA}$ flux and R_{TOA} are calculated by the NASA Langley modified Fu-Liou RTM by using ARM merged soundings as input for each case. The ARM and CERES Ed2 and Ed4 retrieved r_e and τ, ARM-measured cloud base and cloud top heights, and R_{sfc} from each case, as well as the domain mean albedos, are also used as input for the RTM during calculation. The climatic mean aerosol optical depth (0.05) is used for both snow and snow-free cases in this study. The calculated SW fluxes, transmissivity γ and R_{TOA}, respectively, are then compared with the collocated ARM surface and CERES TOA observations to provide a consistency check to the ARM and CERES Ed2 and Ed4 retrieved cloud microphysical properties.

2.4 Domain Representativeness of the ARM NSA PSP-Measured Surface Albedo

The measured daily broadband R_{sfc} values at the ARM NSA site remain nearly constant from late February to late May (~0.8), then drop significantly to 0.16 around the middle of June until late September, and eventually rise and return to 0.8 around the middle of October [*Dong et al*., 2010]. Because the NSA site is only representative of an area of a few tens of meters, it is inaccurate to use the point observed surface albedo to represent the domain of 30 km × 30 km heterogeneous region. As shown in Figure 1, the area surrounding the ARM NSA site is particularly variable during the transitional seasons. A CERES field of view covers a surface area ranging from a minimum of ~20 km^2 at nadir to ~100 km^2 at shallow viewing angles [*Rutan et al*., 2009]. Although the ARM cloud retrieval algorithm was derived from ARM ground-based observations [*Dong and Mace*, 2003], to make apples-to-apples comparison with the CM cloud retrievals and to perform a radiation closure study for both the surface and TOA radiation budgets, we must use the domain mean albedo in both the ARM cloud retrievals and radiation budget calculations.

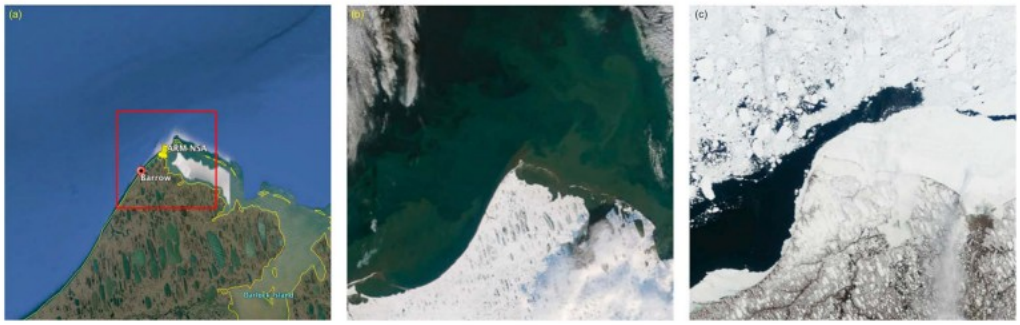

Figure 1. (a) The ARM North Slope of Alaska (NSA) site centered in 100 km × 100 km box; the red box shows the domain of 30 km × 30 km for this study. (b) The MODIS true color image over this region on 22:15 UTC, 13 October 2003; (c) the MODIS true color image on 22:40 UTC, 5 June 2004.

Figure 1a shows that the ARM NSA site is only 1.6 km from the coast. The ARM up- and down-looking standard Eppley precision spectral pyranometers (PSPs) provide measurements of hemispheric downward and upward broadband shortwave (SW, 0.3–3 μm) fluxes at the surface, respectively. Approximately 80% of the downward SW flux measured by the pyranometer comes from a circular area of radius equal to cloud base height, centered directly above the pyranometer. For low-level stratiform clouds over the ARM NSA site, most of the cloud base heights range from 0.5 km to 1 km [*Qiu et al.*, 2015]. Thus, the primary cloud area affecting the pyranometer measurements ranges from 0.8 km^2 to 3 km^2 with a maximum diameter of 2 km. It is reasonable to assume that cloud properties on such a scale are horizontally homogeneous for an overcast cloud layer. Therefore, the $SW^{\downarrow}_{sfc}$ fluxes and the $SW^{\uparrow}_{sfc}$ fluxes (only affected by a few tens of meters near the ARM NSA site) measured by ARM PSPs primarily represent the land surfaces nearby the ARM NSA site with minor contributions from the ocean and nearby large ponds and a lagoon. However, the contributions from clouds over the darker areas will tend to reduce γ and not R_{sfc}, so that r_e (τ) will be biased low (high) when computed with equation 1a. The magnitude of the biases depends on cloud base height and how much open water or thin ice is present along the coast. The CM cloud retrievals and the TOA reflected SW fluxes, especially, are also affected by the ocean and land surface distribution over the domain. In order to perform a radiation closure study at both the surface and TOA over the entire domain, the surface albedo must be adjusted. The ARM PSP-measured surface albedo represents the upper limit for the domain, while the ocean albedo ($R_{sfc} \sim 0.06$) represents the lower limit in calculating the surface and TOA radiation budgets.

For snow-free cases, open water including the lagoon covers 58.3% of the domain and the land covers 41.7% (Figure 1a). Using 0.16 from the ARM PSP-measured surface albedo and assuming 0.06 for the ocean surface albedo, the domain mean surface albedo is estimated to be ~0.102 ($0.583 \times 0.06 + 0.417 \times 0.16$), which is 63.6% of the ARM measurements. This value is used in the snow-free ARM cloud property retrievals and surface and TOA radiation budget calculations in this study.

The cloud property retrievals and the surface and TOA radiation budgets are significantly affected by surface albedo [*Dong and Mace*, 2003]. Because the surface characteristics of the ARM NSA site and environs change significantly during spring (from mid-May to mid-June) and early autumn (from mid-September to mid-October), it is important to consider the changes in surface albedo. During these two transitional time periods, the land is covered by snow ($R_{sfc} \sim 0.8$ measured by ARM PSPs), whereas the surfaces within the domain are highly variable with the following three conditions: (1) the ocean is wide open (Figure 1b), (2) the ocean has open leads (Figure 1c), and (3) the ocean is covered by sea ice or snow with albedos similar to the ARM PSP measurements (not shown).

For snow condition (1), if the lagoon is not frozen (mostly occurs from mid-September to late October when the ARM NSA site is often covered by snow), the domain mean albedo will be ~0.369 ($0.417 \times 0.8 + 0.583 \times 0.06$) if the ARM PSP-measured R_{sfc} is ~0.8 and R_{ocean} is still 0.06, which is 46% of the ARM PSP-measured surface albedo. This scenario is the lower limit for snow-covered conditions and will be used in Table 3 for a sensitivity study.

In the spring, leads often open up around Barrow, when the Beaufort Sea is normally under high pressure that produces strong winds, which cause large cracks in the ice pack and push ice away from the Alaskan and Canadian coasts (e.g., http://neven1.typepad.com/blog/cracks-and-leads/). It is likely that open water and/or at least dark thin ice over water often covers a portion of the domain, particularly along the coast around Barrow when the ARM NSA site is covered by snow (e.g., Figure 1c). If the lagoon and ponds over the land are frozen and covered by snow or ice and the ocean is 100% open, the open water covers 48.4% of the domain and the land is 51.6%. The domain mean albedo will be ~0.442 ($0.516 \times 0.8 + 0.484 \times 0.06$). This scenario represents the lower limit for snow condition (2) and the ARM PSP-measured R_{sfc} (~0.8) represents the upper limit. Therefore, the actual domain albedos will fall between these two extremes. The average of the lower (0.442) and upper (0.8) limits, 0.621, is used as the domain mean albedo for the condition (2) during the period of May–June in this study.

For snow condition (3), when the ocean is covered by sea ice or snow, the domain mean albedo should be close to the ARM PSP measurement (~0.8) during the period of March–April. With a total of 108 Terra cases and 106 Aqua cases in this study, the winter cases (from March–April, $R_{sfc} \sim 0.8$) are 56 (26.2% of 214), the spring cases (May–June, $R_{sfc} \sim 0.621$) are 136 (63.6%), and the autumn cases (from September–October, $R_{sfc} \sim 0.369$) are 22 (10.3%). The weighted domain mean albedo will be 0.642 ($0.8 \times 0.262 + 0.621 \times 0.636 + 0.369 \times 0.1$) for all cases. This weighted domain average is 80% (0.642/0.8) of the ARM PSP-measured albedo. Clear skies over this small region are very rare in snow-covered conditions, so it is not possible to monitor the domain clear-sky albedo with any certainty. Therefore, a surface albedo equivalent to 80% of that measured at the ARM site is used in this study to calculate the domain ARM cloud property retrievals and surface and

TOA radiation budgets for snow cases. We accept that this fixed percentage of 80% may lead to relatively large variations in some individual cases in the ARM cloud property retrievals and radiation calculations; however, this is our best estimate for the domain mean albedo without knowing the actual coverage of open water for each case. In this study, we focus more on statistical comparisons from the averages in the tables, not on individual cases.

3 Results and Discussions

The cases used in this study were selected from the ARM radar-lidar observations and satellite retrievals. As a result, a total of 206 Terra and 140 Aqua snow-free cases ($R_{sfc} \leq 0.3$) and 108 Terra and 106 Aqua snow cases ($R_{sfc} > 0.3$) over the ARM NSA site were selected from March 2000 to December 2006. The criteria used to select these cases have been discussed in *Dong et al.* [2008] and *Xi et al.* [2014] and summarized as follows: a continuous, single-layer and overcast cloud layer without overhead cirrus clouds or clear-sky pixels was identified from both surface and satellite observations. Therefore, the following results only represent the single-layered overcast liquid-phase and liquid dominant mixed-phase Arctic stratus clouds at the ARM NSA site.

3.1 Cloud Microphysics

3.1.1 Snow-Free Cases

Figure 2 shows the time series of ARM and CERES Ed4/Ed2 retrieved cloud-droplet effective radius (r_e), optical depth (τ), and cloud liquid water path (LWP) at the ARM NSA site with the sample number in order from March 2000 to December 2006 for Terra cases and July 2002 to December 2006 for Aqua cases. The scatterplots and probability distribution functions (PDFs), as well as their statistical results, are shown in Figures 3 and 4. The comparisons in Figure 2 represent the spatially averaged satellite results (30 km × 30 km) and temporally (1 h) averaged ground-based retrievals. However, the r_e comparison involves an additional error source because the satellite-retrieved r_e (e.g., using 3.7 μm channel) is representative of cloud particle size near the cloud top for optically thick clouds [e.g., *Nakajima and King*, 1990], while the surface-retrieved r_e, weighted by water mass in the cloud, represents the layer mean particle size. Theoretically, r_e values should increase from cloud base to cloud top assuming adiabatic growth [e.g., *Miles et al.*, 2000], and the CERES Ed4 and Ed2 retrieved r_e values should be larger than the layer mean ARM r_e retrievals.

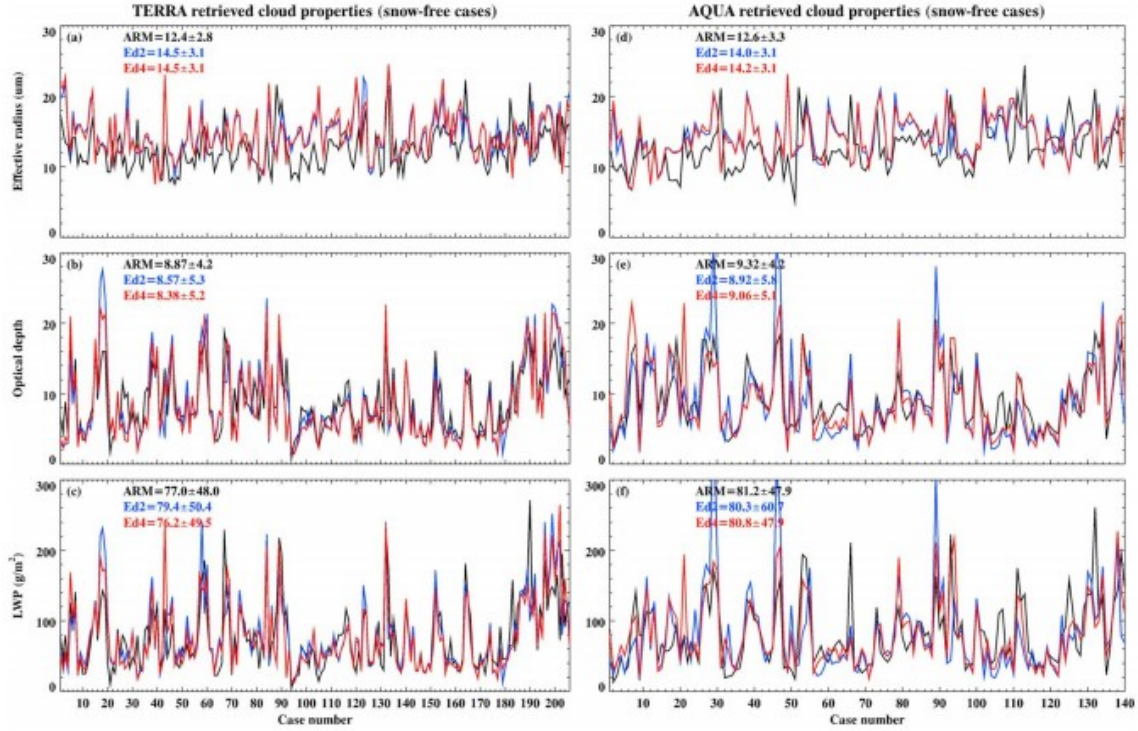

Figure 2. Time series of ARM retrieved (a) cloud-droplet effective radius r_e, (b) optical depth τ, and (c) *LWP* (1 h average) and matched Terra CERES Edition 2 (Ed2) and Edition 4 (Ed4) cloud microphysical retrievals (30 km × 30 km) for daytime single-layer and overcast stratus clouds over the ARM NSA site (sample number is ordered from March 2000 to December 2006). (d–f) The same as Figures 2a–2c except for Aqua cases from July 2002 to December 2006. A total of 206 snow-free ($R_{sfc} \leq 0.3$) Terra cases and 140 Aqua cases were selected, respectively, for this study.

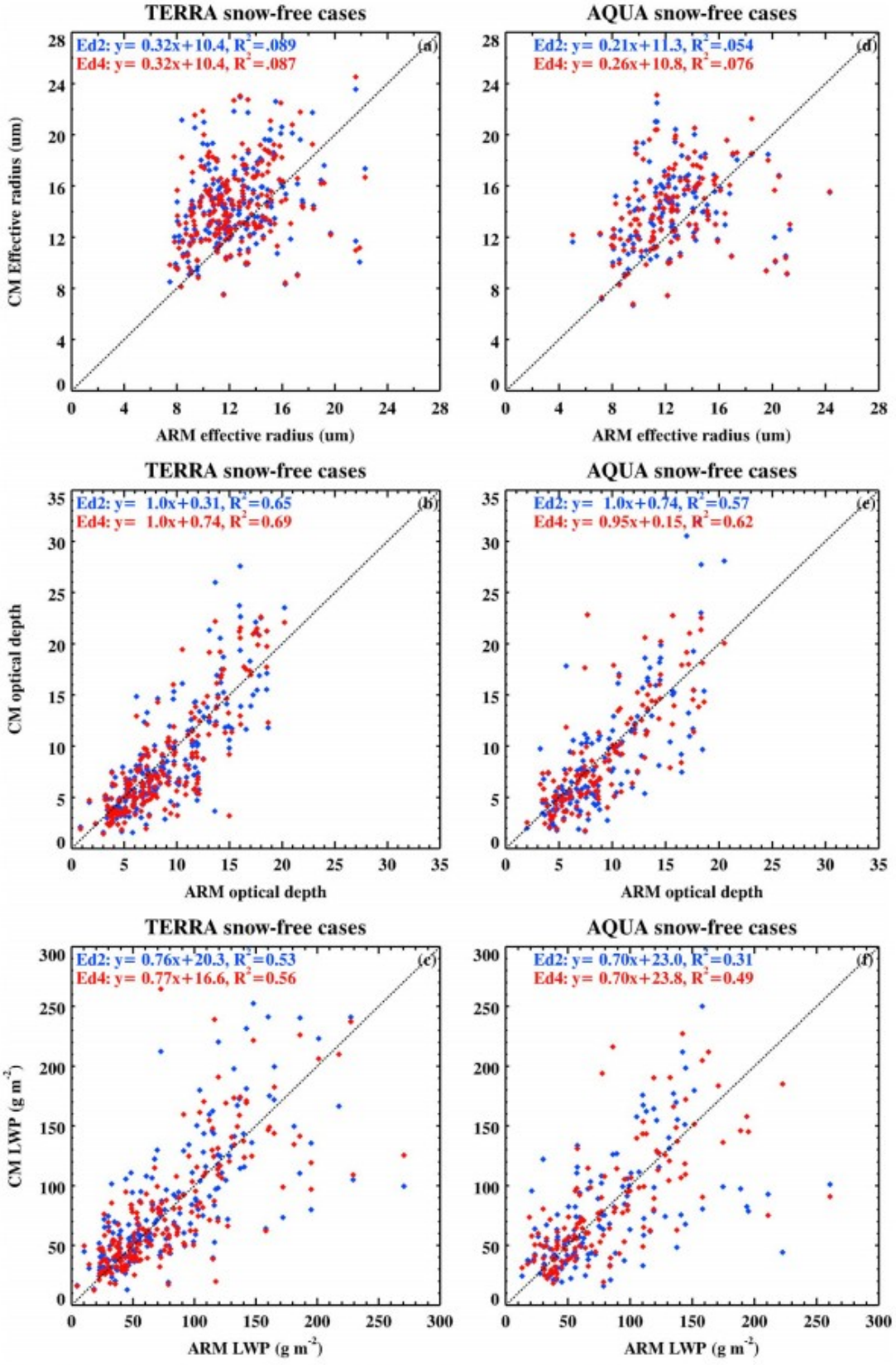

Figure 3. Same as Figure 2 except for scatterplots of (a–c) Terra cases and (d–f) for Aqua cases.

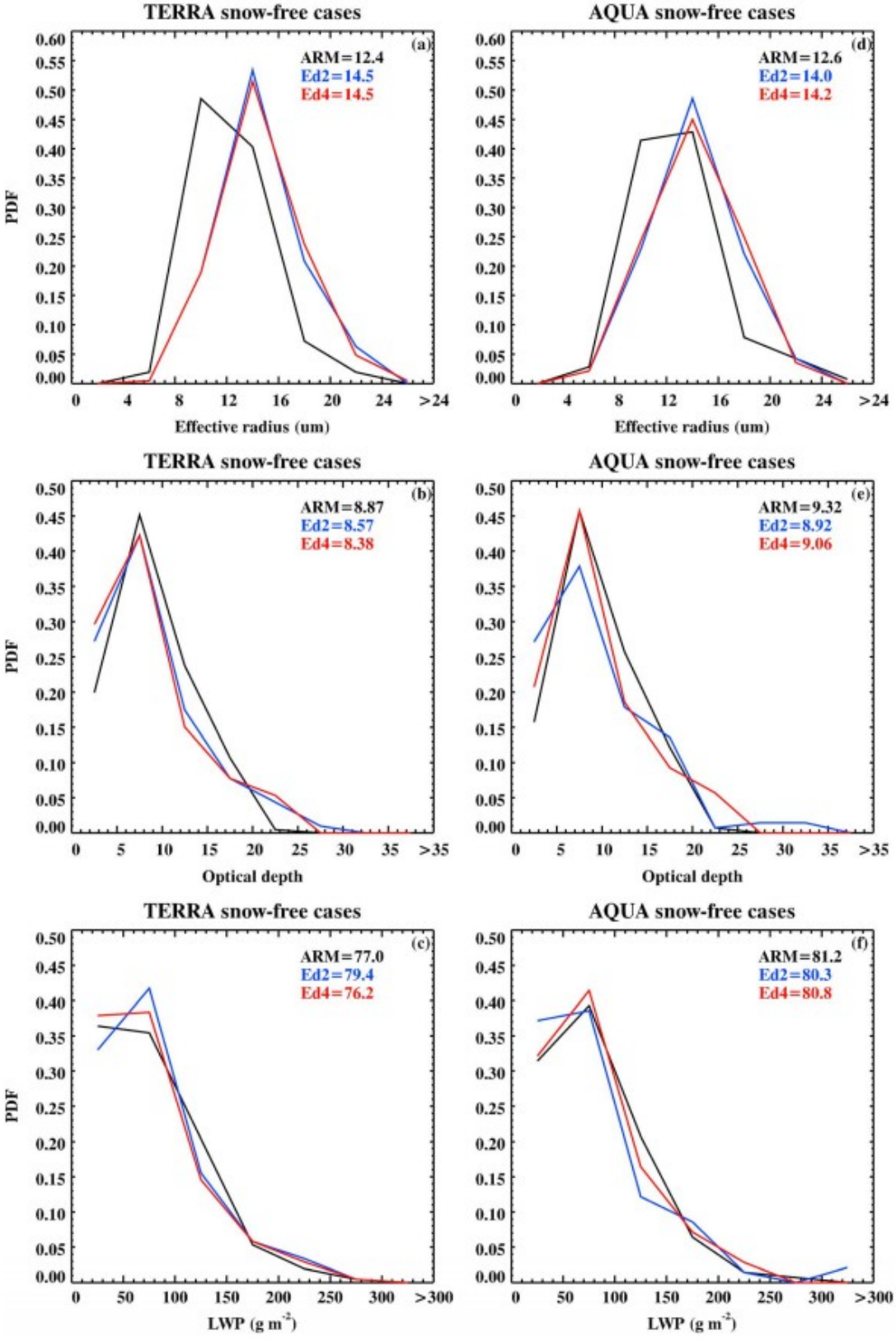

Figure 4. Same as Figure 3 except for probability distribution functions (PDFs).

As shown in Figures 2a and 2d, the Terra and Aqua Ed4 and Ed2 r_e values are almost indistinguishable, but their mean values are $1 \sim 2$ μm greater than their ARM counterparts. Figures 3a and 3d show that most of the Terra and Aqua Ed4/Ed2 r_e retrievals are greater than the ARM results with very low correlation coefficients ($R^2 = 0.054$–0.089). The probability distribution function (PDFs) of the Terra and Aqua Ed4/Ed2 r_e retrievals shift to large values with mode values of 14 μm, about 4 μm greater than the ARM mode values (Figures 4a and 4d). Based on these statistical results, we can conclude that the Ed4 and Ed2 r_e retrievals from both Terra and Aqua are the same and their mean values are 1.8 μm greater than the ARM ones, which is consistent with the theoretical discussions.

The τ and *LWP* comparisons are presented in Figures 2b and 2c and 2e and 2f for the Terra and Aqua cases, respectively. Their corresponding scatterplots and PDFs are given in Figures 3b and 3c and 4e and 4f. As demonstrated in Figures 2-4, most of Ed4 and Ed2 τ values are in excellent agreement with the ARM results, with close means (Ed4 = 8.4 and Ed2 = 8.6 versus ARM = 8.9 for Terra, 9.1 and 8.9 versus 9.3 for Aqua) and moderate correlations ($R^2 = 0.57$–0.69). Similar to their r_e comparisons, the τ differences between Ed4 and Ed2 are also very small for both satellites, indicating that there are no significant changes in the τ retrievals between the two algorithms for snow-free cases. The good agreement in *LWP* between Ed4/Ed2 and ARM results is due to excellent agreement in their τ values, as well as the good r_e comparisons. The correlations between Ed4/Ed2 and ARM *LWPs* from both Terra and Aqua are slightly lower than those for the τ values, but much greater than for the r_e values. This is understandable because the CERES *LWP* is computed as a product of the CERES τ and r_e retrievals.

The statistical results are summarized in the top half of Table 1, which provides the correlation coefficients, R, and the standard deviations of the differences, SDD, for each parameter. For instance, the Aqua and Terra differences relative to the ARM r_e retrievals are 1.5 ± 3.9 μm and 2.1 ± 3.5 μm, respectively, for the two editions. The uncertainties in τ are -0.4 ± 3.0 for Terra and -0.3 ± 3.5 for Aqua relative to the ARM retrievals, with slightly smaller SDDs for the Ed4 results. Uncertainties in the Terra and Aqua *LWP* retrievals are 0.8 ± 35.3 g m^{-2} and -0.6 ± 44.6 g m^{-2}, respectively, again, with smaller SDDs for the Ed4 retrievals. Overall, the Ed4 *LWP* SDD values translate to relative uncertainties of 45% compared to ~56% for the Ed2 results.

Table 1. Means and Standard Deviations of Differences (SDD) and Linear Correlation Coefficients (R) of MODIS Cloud Microphysical Property Retrievals Relative to Surface Results for Snow-Free and Snow Cases

			CERES-ARM				CERES-ARM				CERES-ARM		
Snow-Free Cases		r_e Mean	Mean	SDD	R	τ Mean	Mean	SDD	R	LWP Mean	Mean	SDD	R
Terra (206)	ARM	12.4				8.87				77.0			
	Ed2	14.5	2.1	3.53	0.30	8.57	−0.30	3.12	0.81	79.4	2.4	36.2	0.73
	Ed4	14.5	2.1	3.55	0.29	8.38	−0.49	2.90	0.83	76.2	−0.8	34.5	0.75
Aqua (140)	ARM	12.6				9.32				81.2			
	Ed2	14.0	1.4	3.99	0.23	8.92	−0.40	3.82	0.75	80.3	−0.9	52.4	0.56
	Ed4	14.2	1.6	3.91	0.27	9.06	−0.26	3.18	0.79	80.8	−0.4	36.9	0.70
			CERES-ARM				CERES-ARM				CERES-ARM		
Snow cases		r_e Mean	Mean	SDD	R	τ Mean	Mean	SDD	R	LWP Mean	Mean	SDD	R
Terra (108)	ARM	11.1				7.05				58.1			
	Ed2	12.8	1.7	3.58	0.47	8.16	1.11	2.55	0.78	70.3	12.2	33.5	0.72
	Ed4	12.8	1.7	3.41	0.49	7.93	0.88	4.38	0.64	67.0	8.9	42.3	0.64
Aqua (106)	ARM	11.7				7.81				69.0			
	Ed2	13.1	1.4	4.08	0.49	5.84	−1.97	3.69	0.50	51.1	−17.9	51.7	0.46
	Ed4	13.2	1.5	4.17	0.48	8.19	0.38	4.39	0.63	71.2	2.2	53.2	0.54

Since *LWP* is a product of τ and r_e, the CERES *LWP* errors will result from errors in CERES τ and r_e retrievals, as seen for a few outliners in Figures 2c and 2f. Errors in either variable can offset the other leading to a good estimate of *LWP* or they can compound each other leading to extreme errors. For example, both Ed4 and Ed2 *LWPs* in Terra case 18 are much larger than ARM *LWP*, primarily due to their large τ retrievals, while their r_e retrievals agree well with the ARM r_e. On the other hand, both Ed4 and Ed2 r_e retrievals in Terra case 43 are nearly double the ARM value, but their different τ retrievals (Ed4 is close to ARM τ but Ed2 is much less) result in different *LWPs*. For Aqua cases 27, 43, and 89, Ed4 *LWPs* are close to ARM *LWPs*, but Ed2 *LWPs* are much larger due to their large τ retrievals. Both Ed4 and Ed2 r_e retrievals in these three cases are nearly identical, and slightly greater than the ARM ones. The ARM *LWPs* in Terra case 190 and Aqua case 132 are much greater than the Ed4 and Ed2 *LWPs* because the ARM r_e retrievals are much larger than the CERES values although their τ retrievals are close to each other. A first check using ARM radar-lidar observations shows that most of these outliers are low-level stratus clouds with no cirrus clouds above. Therefore, it is necessary to investigate these cases in the future.

3.1.2 Cloud Microphysics Over Snow

The time series of ARM and CERES Ed4/Ed2 retrieved r_e, τ, and *LWP* over snow surfaces are shown in Figure 5, and their scatterplots and probability distribution functions (PDFs), as well as their statistical results, are shown in Figures 6 and 7. In general, the r_e, τ, and *LWP* comparisons between CERES Ed4/Ed2 and ARM over snow surfaces agree well each other and are close to their snow-free comparisons with a few exceptions. Both ARM and CERES Ed4/Ed2 retrieved r_e, τ, and *LWP* retrievals over snow surfaces are slightly smaller than their corresponding snow-free counterparts, and CERES Ed2 retrieved τ and *LWP* for Aqua cases over snow surfaces are much lower than ARM and CERES Ed4 retrievals.

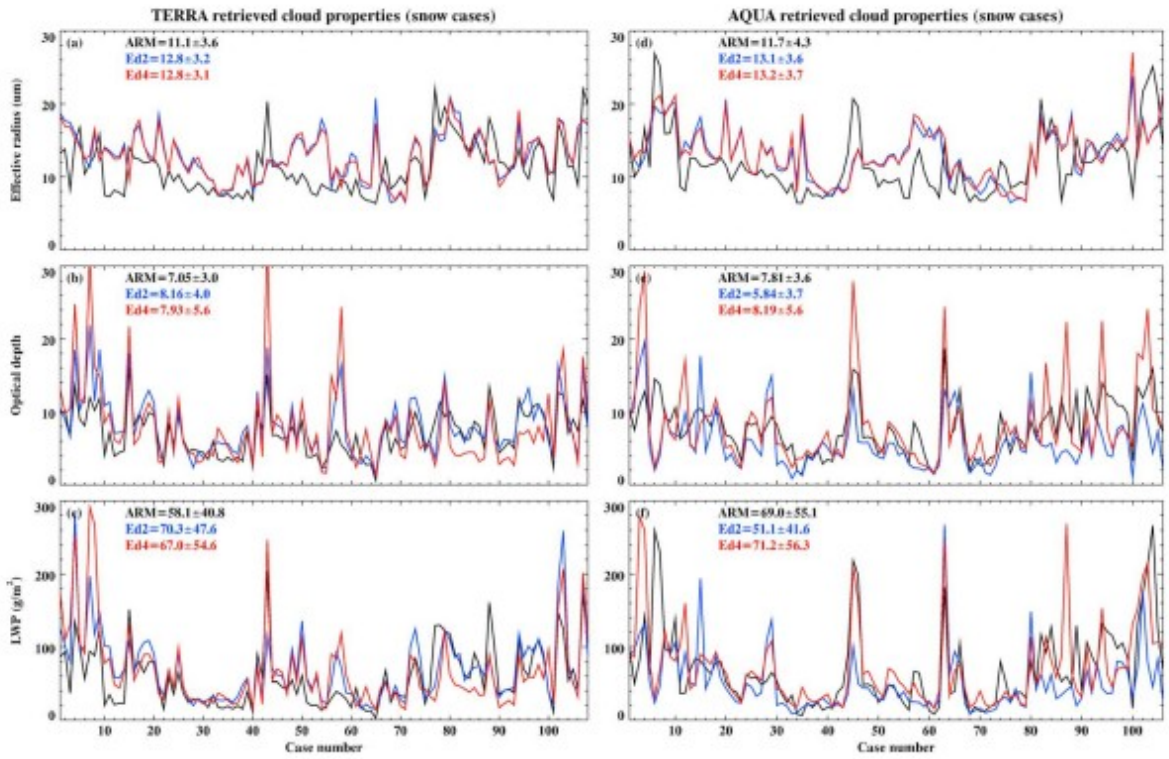

Figure 5. Same as Figure 2 except for snow cases ($R_{sfc} > 0.3$). A total of 108 Terra cases and 106 Aqua cases were selected, respectively, for this study.

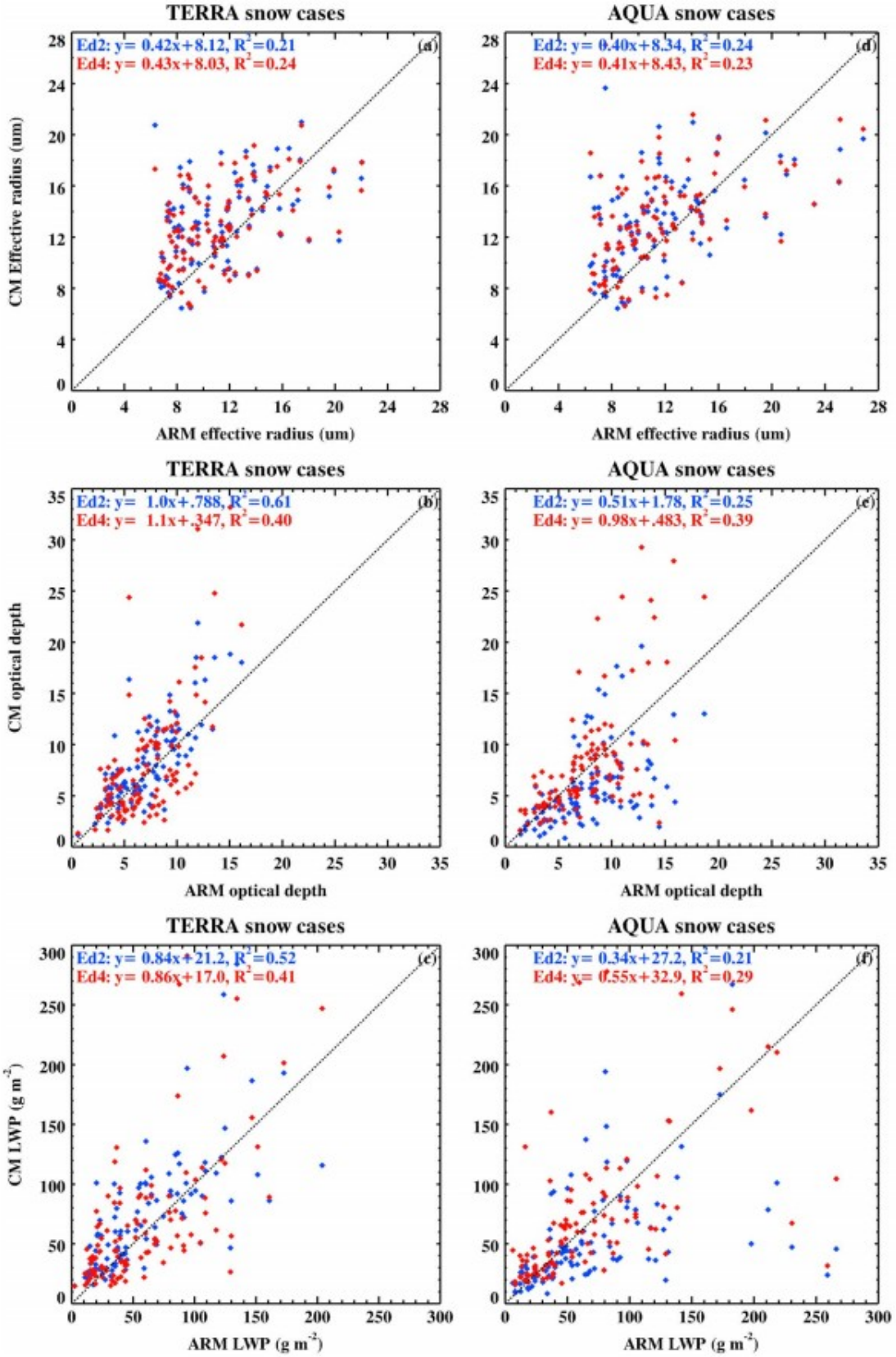

Figure 6. Same as Figure 3 except for snow cases.

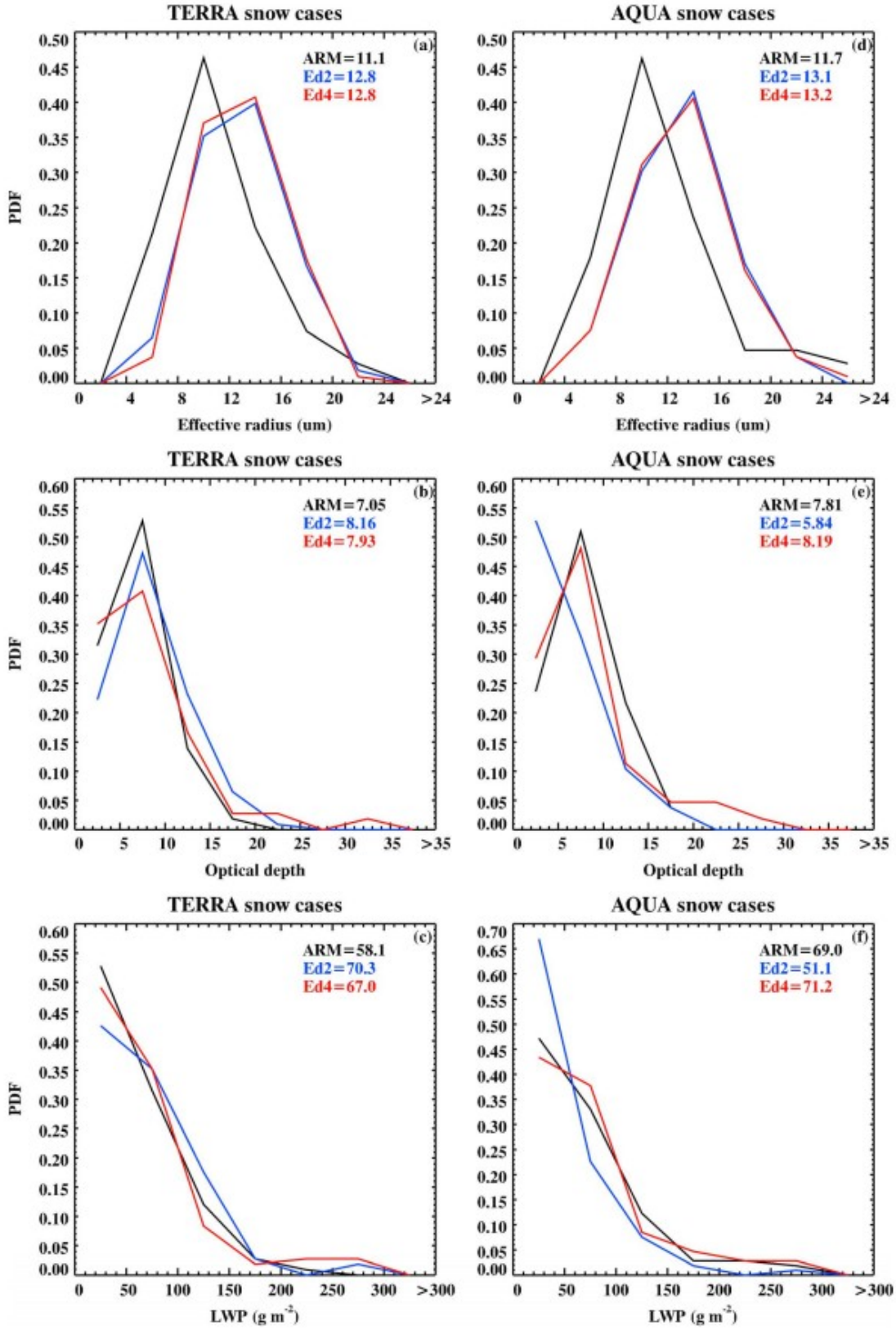

Figure 7. Same as Figure 4 except for snow cases.

The CERES Ed4 and Ed2 r_e retrievals are nearly identical for both Terra (Figure 5a) and Aqua (Figure 5d), and the mean differences between the CERES and ARM are ~1.6 μm (14%), which is close to the snow-free comparisons. Relative to the τ comparisons over snow-free surfaces (Figure 2), the τ differences over snow surfaces are slightly larger, especially for certain cases. Although the CERES Ed4 and Ed2 τ retrievals basically follow the variation of the ARM retrievals (Figures 5b and 5e), the values are, on average, greater (except for Ed2 of Aqua cases) than the ARM retrievals with larger variability, and thus lower correlations ($R^2 = 0.25$–0.61) as shown in Figures 6b and 6e. The averaged Ed4 and Ed2 τ values are 0.88 and 1.11, respectively, greater than the ARM mean (7.05) for Terra cases, and they are 0.38 greater and 1.97 lower than the ARM average (7.81) for Aqua cases with different mode value for Aqua snow cases (Figure 7e). The ARM τ is calculated using equation 1b, and its uncertainty over snow surfaces is also larger than its snow-free counterpart due to large uncertainty in ARM r_e retrievals over snow surfaces.

The CERES Ed2 τ retrieval over snow surfaces is from the shortwave-infrared infrared near-infrared technique (SINT), using 1.6 μm (Terra) or 2.1 μm (Aqua) channels instead of the visible channel in VISST for snow-free surfaces. The Ed4 SINT uses the 1.24 μm channel, which at the time of this writing was operating well on both Terra and Aqua. Snow is more reflective at 1.24 μm, typically having albedos between ~0.3 and 0.4 [e.g., *Chen et al.*, 2010] compared to albedos of less than 0.1 and 0.2 at 2.1 and 1.6 μm, respectively, and between 0.4 and 0.9 at 0.65 μm [*Chen et al.*, 2006]. The small snow/ice albedos at 1.6 and 2.1 μm facilitate relatively accurate retrievals of τ, but the greater absorptivity of the cloud at 1.6 and 2.1 μm limits the maximum optical depth that can be retrieved with these channels to ~25 and ~16, respectively, for liquid clouds [*Minnis et al.*, 2010b]. Smaller absorptivity at 1.24 μm permits retrieval of greater range of optical depths, but the smaller contrast of the cloud and surface increases the potential for greater uncertainty if the surface albedo is not accurately characterized. The difference in the spectral dependency of the limitations is most evident in Figure 5e, which shows that the Ed4 optical depths are often greater than the 2.1 μm Ed2 retrievals, especially for $\tau > 20$. There is less difference between the Terra 1.6 μm Ed2 and 1.24 μm Ed4 retrievals (Figure 5b), except for the few instances when $\tau > 20$. On the other hand, some of the Ed4 retrievals are less than their Ed2 counterparts for smaller τ values (e.g., samples 81–93 in Figure 5b), possibly as the result of the greater uncertainty in the surface albedo. The histograms in Figures 7b and 7e provide further demonstration of the limitations and uncertainties. The Ed4 values yield a greater range, while the 2.1 μm Ed2 retrievals are skewed to the smallest range.

The *LWP* comparisons between Ed4/Ed2 and ARM retrievals in Figures 5-7 are similar to the τ comparisons. Most of the Ed4 and Ed2 *LWPs* scatter around the ARM *LWPs* except for a few large outliners identified by the large

biases in τ retrievals, such as Terra cases 4, 7, 43, and 103 and Aqua cases 3, 45, and 87. For the Terra cases, the Ed4 and Ed2 retrieved *LWPs*, on average, are 8.9 and 12.2 g m^{-2} higher than the ARM mean (58.1 g m^{-2}). The *LWP* means from Ed4, Ed2, and ARM for Aqua cases are 71.2, 51.1, and 69.0 g m^{-2}, respectively. The negative bias of −17.9 g m^{-2} for Aqua Ed2 is primarily due to its smaller optical depths (Figures 7e and 7f).

The comparisons over snow are summarized in the bottom half of Table 1. The CERES biases and SDDs in r_e are close to their snow-free counterparts with slight higher correlations. For τ, the magnitudes of the bias increase, overall, from ~4% in snow-free conditions to 20% and 9% over snow for Ed2 and Ed4, respectively, but their SDDs and *R* values are comparable. The magnitudes of the Ed2 *LWP* biases are much larger over snow, but if the results from both satellites together are considered, they are nearly zero because of the opposite signs. Since the Ed4 Terra and Aqua results use the same channel for retrieving τ over snow, their results can be combined to provide a best estimate error in *LWP* over snow of 9 ± 75% relative to the microwave radiometer retrieval. The mean Ed2 *LWP* SDDs are only 58% and 75% for Terra and Aqua, respectively, confirming that the use of the 1.24 μm channel gives a smaller bias than the other channels, but with overall slightly greater instantaneous uncertainty.

3.1.3 Sensitivities of the Retrieved Cloud Properties to *SZA* and R_{sfc}

To further examine the results, the individual values of *LWP*, τ, and r_e for both the Terra and Aqua cases were averaged in discrete bins of SZA and surface albedo (R_{sfc}). Figure 8 shows the histograms of the three variables as a function of SZA. The ARM mean *LWPs* do not vary monotonically with SZA for either snow-free (Figure 8a) or snow conditions (Figure 8b). In the absence of snow, the CERES mean *LWPs* increase with SZA, particularly for SZA > 78°. However, in relative terms, the CERES Ed4 values track the ARM means well, except for the last SZA bin for all surface conditions. For snow-free cases, the ARM r_e values decrease from 14 to 12 μm with increased SZA from 48° to 78° (Figure 8c), while the CERES r_e means are relatively constant, except for the last bin. The results of these variations produce good agreement (<2 μm) between the surface and satellite r_e values for SZA < 72°, but steady divergence of the values as SZA increases. Over snow (Figure 8d), both CERES and ARM r_e values are less dependent on SZA, and their differences are even smaller than their snow-free counterparts. The Ed4 and Ed2 values remain close for both conditions. All retrieved optical depths increase with SZA over snow-free surfaces (Figure 8e) similar to the *LWP* data, except that the ARM values are close to the CERES means in all bins. Over snow (Figure 8f), both CERES and ARM retrieved τ values decrease with SZA, and then increase in the last two bins. Both Ed4/Ed2 τ values agree well with ARM values in the first three bins, but only Ed4 agrees with ARM in the bin 4 and Ed2 agrees with ARM in the last bin.

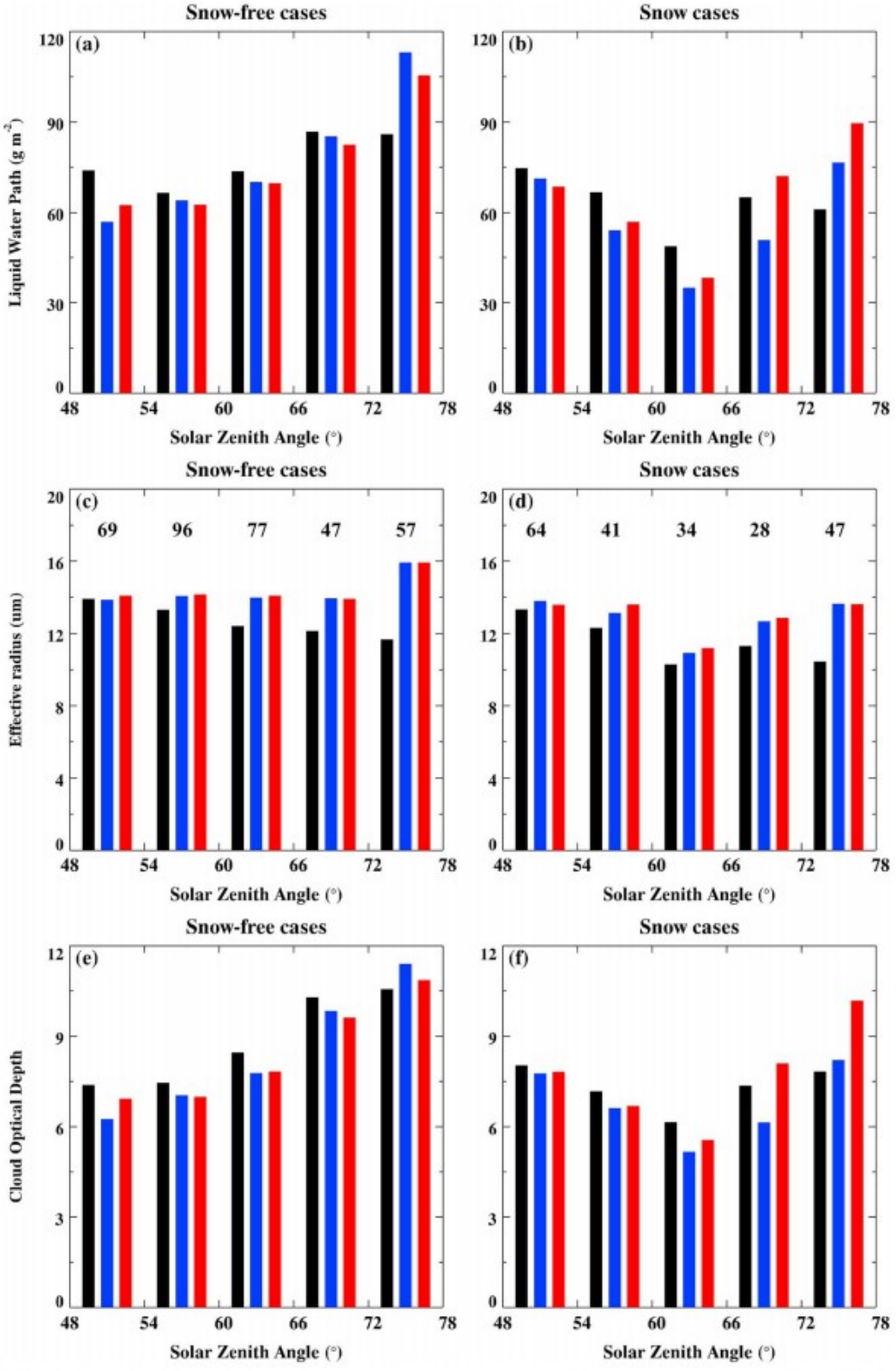

Figure 8. Variation of mean cloud (a and b) liquid water path, (c and d) droplet effective radius, and (e and f) optical depth with solar zenith angle for (left column) snow-free and (right column) snow-covered surfaces. The numbers of samples in each bin are shown in Figures 8c and 8d.

The same parameters were averaged as a function of the ARM surface albedo resulting in the histograms plotted in Figure 9. The mean *LWPs* in Ed4/Ed2 agree with ARM means within 10 g m^{-2} for all bins (Figure 9a) except for the bin 2 ($R_{sfc} = 0.2$–0.4), where the ARM mean *LWP* is ~20 g m^{-2} less than Ed4/Ed2 values. The r_e differences between Ed4/Ed2 and ARM retrievals basically follow their *LWP* differences, most of them are less than 2 μm except for the bin 2 ($\Delta r_e \sim 4$ μm; Figure 9b). All retrieved optical depths decrease slightly with R_{sfc} except for Ed4 retrieval in the last bin. In general, both CERES and ARM retrievals have similar dependencies on R_{sfc} and agree very well each other except for *LWP* and r_e in bin 2 and for Ed4 τ in the last bin.

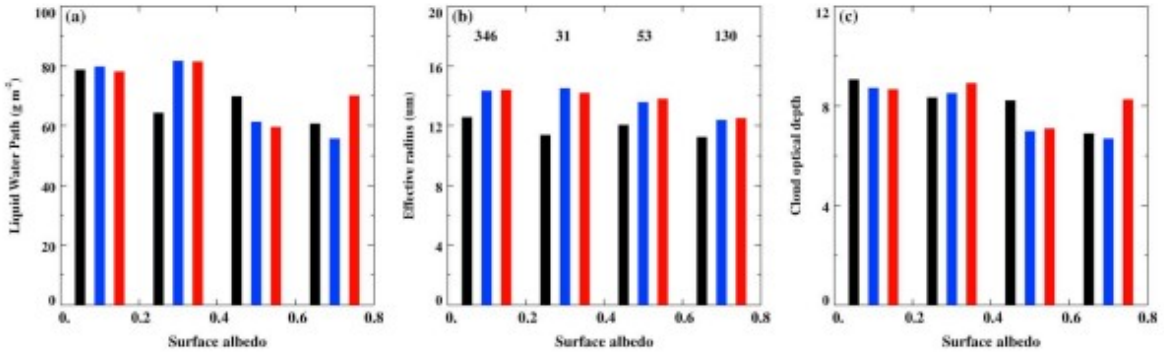

Figure 9. Variation of mean cloud (a) liquid water path, (b) droplet effective radius, and (c) optical depth with ARM surface albedo for combined snow-free and snow-covered surfaces. Number of samples in each bin is shown in Figure 9b.

3.2 Radiation Closure Study

Given the encouraging agreement in the ARM and CERES Ed4/Ed2 cloud retrievals, there is a question of how well the RTM calculations using these cloud retrievals as input agree with both surface and satellite SW observations over the domain. To answer this question, the ARM and CERES Ed4/Ed2 retrieved r_e and τ values, as well as ARM radar-lidar derived cloud base and cloud top heights and adjusted R_{sfc} (63.6% of the ARM PSP-measured R_{sfc} for snow-free cases and 80% for snow cases are used to represent the domain mean albedos in this study) for each case, are used as input for the NASA Langley modified Fu-Liou radiative transfer model (RTM). The RTM calculated $SW^{\downarrow}_{sfc}$ flux and γ at the surface and $SW^{\uparrow}_{TOA}$, and R_{TOA} are then compared with the collocated ARM surface and CERES TOA observations.

3.2.1 Radiation Closure Study Over Snow-Free Surfaces

The comparisons of $SW^{\downarrow}_{sfc}$ flux and γ between the RTM calculations and ARM surface PSP observations are illustrated in Figures 10a and 10b for Terra and Figures 10 and 10f for Aqua, and their scatterplots with the statistics are presented in Figures 11a and 11c. Using the ARM and Terra Ed4/Ed2 cloud retrievals as input, the calculated $SW^{\downarrow}_{sfc}$ fluxes are, on average, −2.8 W

m^{-2} less and 7.5/4.7 W m^{-2} greater, respectively, than the ARM PSP-measured $SW^{\downarrow}_{sfc}$ flux (210.1 W m^{-2}). For the Aqua comparisons, the mean ARM and Ed4/Ed2 computed $SW^{\downarrow}_{sfc}$ fluxes, on average, are −0.9 W m^{-2} less and 7.0/13.6 W m^{-2} greater than their PSP-measured counterpart (207.3 W m^{-2}). As shown in Figures 10a and 10e and listed in the top half of Table 2, the average difference in ARM PSP-observed $SW^{\downarrow}_{sfc}$ fluxes between Terra and Aqua cases is 2.8 W m^{-2}, the differences in RTM results between the Terra and Aqua cases are also within a few W m^{-2}, which are consistent with their τ comparisons. The minimum differences between ARM observations and the Fu-Liou RTM calculations using the ARM retrieval as input are understandable because the ARM-observed $SW^{\downarrow}_{sfc}$ flux is used as a constraint during ARM r_e retrievals [*Dong and Mace*, 2003]. This excellent agreement has provided a consistency check to the ARM cloud property retrievals where a δ2-stream radiative transfer model was employed. The RTM-calculated $SW^{\downarrow}_{sfc}$ fluxes using Ed4/Ed2 cloud retrievals for both Terra and Aqua, on average, are 8.2 W m^{-2} (+3.9%) higher than the ARM PSP observations, which makes physical sense since their optical depths are slightly smaller than the ARM τ retrievals (−4.1%).

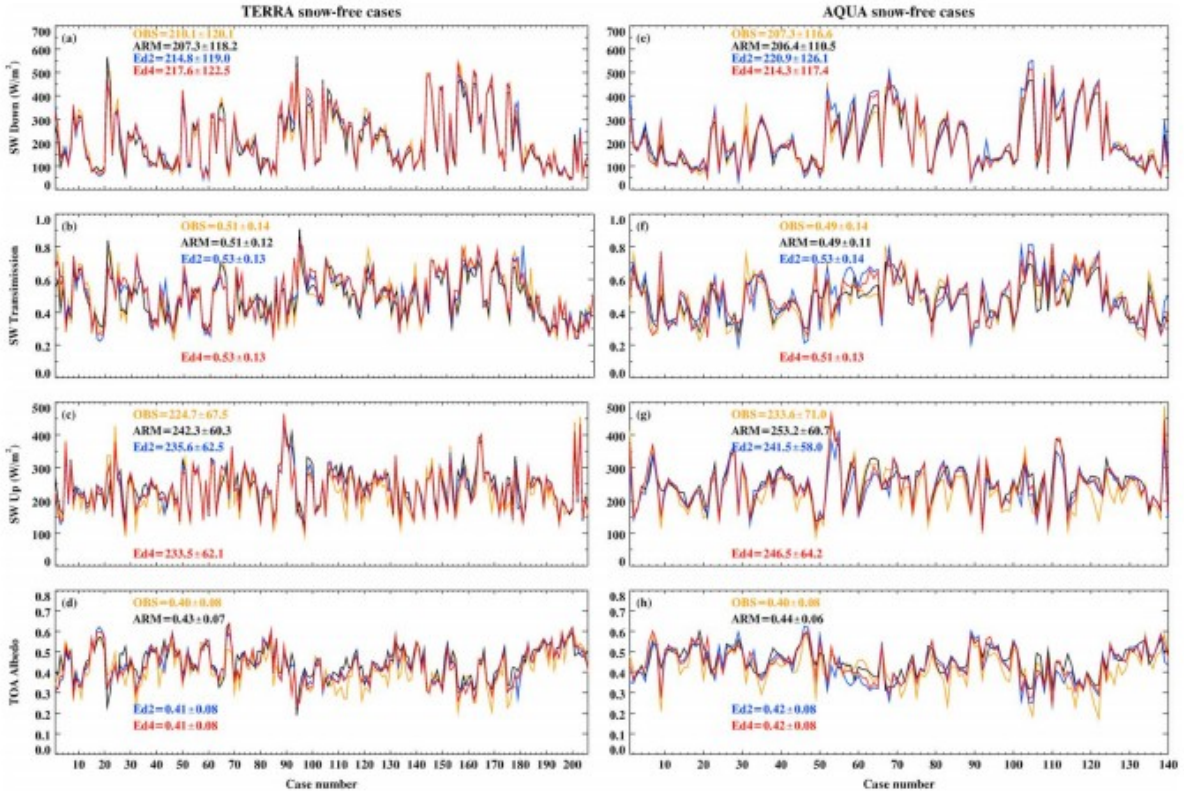

Figure 10. Fu-Liou RTM calculated (a) $SW^{\downarrow}_{sfc}$ flux and (b) transmission γ at the surface and (c) $SW^{\uparrow}_{TOA}$ flux and (d) albedo R_{TOA} with input of ARM, CERES Ed2 and Ed4 retrieved r_e, and optical depth. The corresponding observations (OBS) are the ARM PSP surface measurements and the CERES Single Scanner Footprint (SSF) instantaneous reflected SW flux at the TOA. (e–h) for Aqua cases.

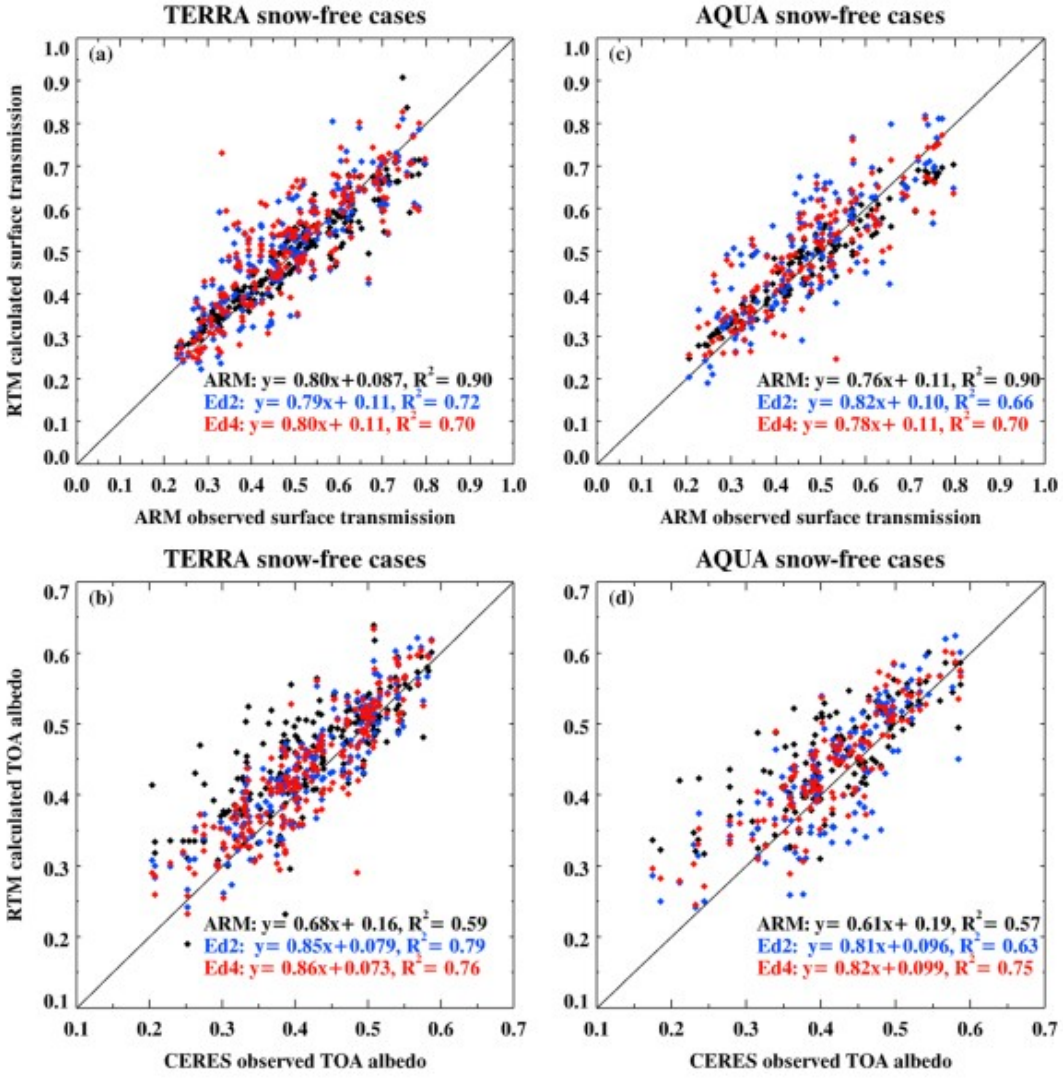

Figure 11. Scatterplots of γ and R_{TOA} for (a and b) Terra cases and (c and d) for Aqua cases.

Table 2. Same as Table 1, But for RTM-Calculated Radiative Properties With Input of Cloud Property Retrievals From Both Surface and Terra and Aqua for Snow-Free and Snow Cases

					RTM-OBS			RTM-OBS			RTM-OBS			RTM-OBS	
Snow-Free Cases		TOA $SW^{\downarrow}$	SFC $SW^{\downarrow}_{clr}$	TOA $SW^{\uparrow}$	Mean	SDD	R_{TOA}	Mean	SDD	SFC $SW^{\downarrow}_{cly}$	Mean	SDD	γ	Mean	SDD
Terra (206)	OBS	559.7	406.2	224.7			0.40			210.1			0.51		
	ARM	561.4	404.6	242.3	17.6	32.9	0.43	0.03	0.06	207.3	−2.8	21.5	0.51	0.002	0.05
	Ed2			235.6	10.9	23.5	0.41	0.01	0.04	214.8	4.7	31.3	0.53	0.02	0.08
	Ed4			233.5	8.8	26.3	0.41	0.01	0.04	217.6	7.5	35.4	0.53	0.02	0.08
Aqua (140)	OBS	573.2	415.2	233.6			0.40			207.3			0.49		
	ARM	574.8	416.1	253.2	19.6	33.2	0.44	0.04	0.05	206.4	−0.9	22.1	0.49	0.002	0.05
	Ed2			241.5	7.9	35.3	0.42	0.02	0.05	220.9	13.6	39.5	0.53	0.04	0.09
	Ed4			246.5	12.9	25.8	0.42	0.02	0.04	214.3	7.0	31.2	0.51	0.02	0.08
					RTM-OBS			RTM-OBS			RTM-OBS			RTM-OBS	
Snow cases		TOA $SW^{\downarrow}$	SFC $SW^{\downarrow}_{clr}$	TOA $SW^{\uparrow}$	Nean	SDD	R_{TOA}	Mean	SDD	SFC $SW^{\downarrow}_{cly}$	Mean	SDD	γ	Mean	SDD
Terra (108)	OBS	551.7	425.2	297.2			0.53			279.0			0.65		
	ARM	553.3	418.1	307.3	10.1	24.9	0.55	0.02	0.05	273.0	−6.0	28.4	0.65	−0.007	0.05
	Ed2			309.4	12.2	22.2	0.55	0.02	0.04	264.4	−14.6	32.4	0.63	−0.03	0.06
	Ed4			305.8	8.6	23.9	0.55	0.02	0.05	274.4	−4.6	42.2	0.65	−0.01	0.09
Aqua (106)	OBS	574.7	440.7	301.7			0.52			278.0			0.63		
	ARM	576.6	437.7	316.4	14.7	29.6	0.54	0.02	0.05	281.0	3.0	29.9	0.64	0.01	0.05
	Ed2			306.9	5.2	31.6	0.53	0.01	0.06	305.7	27.7	49.9	0.69	0.06	0.09
	Ed4			313.4	11.7	28.1	0.54	0.02	0.05	284.8	6.8	48.7	0.65	0.02	0.09

As shown in Table 2, the RTM-calculated and ARM-observed clear-sky $SW^{\downarrow}_{sfc}$ fluxes for Terra are, on average, 404.6 W m^{-2} and 406.2 W m^{-2}, respectively, and they are 416.1 W m^{-2} and 415.2 W m^{-2} for Aqua cases. The excellent agreement in clear-sky $SW^{\downarrow}_{sfc}$ flux between the ARM observations and RTM calculations results in nearly identical SW transmission γ values with very high correlations ($R^2 = 0.90$) between the ARM observations and RTM calculations using the ARM cloud retrievals (Figures 10b, 10f, 11a, and 11c). The positive biases of 0.02 in the RTM calculated γ using the Ed4 and Ed2 cloud retrievals and the relatively high correlations ($R^2 = 0.66$–0.72) are also expected. The comparisons of $SW^{\uparrow}_{TOA}$ fluxes and R_{TOA} between the RTM calculations and CERES observations, on the other hand, show that the RTM-calculated $SW^{\uparrow}_{TOA}$ fluxes and R_{TOA} values using the Ed4/Ed2 cloud retrievals have better agreement with the CERES observations and have higher correlations than the RTM calculations using the ARM cloud retrievals. Compared to the CERES TOA observations, the mean RTM-calculated $SW^{\uparrow}_{TOA}$ fluxes and R_{TOA} values using Ed4/Ed2 cloud retrievals are 10.1 W m^{-2} and 0.015 higher, while those using ARM cloud retrievals are 18.6 W m^{-2} and 0.035 higher.

To further explore the flux differences between the RTM calculations and observations, we use the lower limit ($R_{ocean} = 0.06$) and upper limit (ARM PSP-measured R_{sfc}) of surface albedo as the domain albedo and the same cloud retrievals in Figure 2 to calculate the TOA and surface fluxes. The averages are shown in the top half of Table 3. Using the ARM PSP-measured R_{sfc} and ARM cloud retrievals as input, the RTM-calculated $SW^{\downarrow}_{sfc}$ fluxes, as expected, agree very well with the ARM observations, whereas those with input of CM cloud retrievals are much higher. However, using R_{ocean} and CM cloud retrievals as input, the RTM-calculated $SW^{\downarrow}_{sfc}$ fluxes agree with the ARM observations within a few W m^{-2}, indicating that the CM cloud retrievals primarily used the ocean albedo as background. The $SW^{\uparrow}_{TOA}$ flux differences

using R_{ocean} are much less than those using R_{sfc}, and the RTM calculations with input of CM cloud retrievals also agree with the CERES observations within a few W m^{-2}. The radiation comparisons further confirm the CM cloud retrievals over the ocean albedo.

Table 3. Comparisons of the RTM-Calculated Radiative Properties Using ARM PSP-Measured Surface Albedo R_{sfc} and Ocean Albedo R_{ocean} (0.06)

		TOA SW$^{\uparrow}$		R_{TOA}		SFC SW$^{\downarrow}_{cly}$		γ	
Snow-Free Cases		R_{ocean}	R_{sfc}	R_{ocean}	R_{sfc}	R_{ocean}	R_{sfc}	R_{ocean}	R_{sfc}
Terra (206)	OBS	224.7		0.40		210.1		0.51	
	ARM	236.8	249.6	0.42	0.44	203.5	212.8	0.50	0.52
	Ed2	229.8	243.4	0.40	0.43	211.0	220.1	0.52	0.54
	Ed4	227.5	241.5	0.40	0.43	213.8	222.9	0.53	0.54
Aqua (140)	OBS	233.6		0.40		207.3		0.49	
	ARM	248.0	260.5	0.43	0.45	202.6	211.7	0.49	0.50
	Ed2	235.5	249.5	0.40	0.43	217.2	226.3	0.52	0.54
	Ed4	240.9	254.2	0.41	0.44	210.6	219.8	0.50	0.52
		TOA SW$^{\uparrow}$		R_{TOA}		SFC SW$^{\downarrow}_{cly}$		γ	
Snow cases		0.46α	1.0α	0.46α	1.0α	0.46α	1.0α	0.46α	1.0α
Terra (108)	OBS	297.2		0.53		279.0		0.63	
	ARM	265.9	337.9	0.48	0.61	239.8	298.5	0.58	0.71
	Ed2	270.5	338.5	0.49	0.61	230.3	291.1	0.56	0.69
	Ed4	263.9	336.6	0.48	0.60	241.8	299.7	0.59	0.71
Aqua (106)	OBS	301.7		0.52		278.0		0.63	
	ARM	276.0	345.9	0.48	0.60	247.8	306.3	0.57	0.69
	Ed2	259.3	340.4	0.45	0.59	275.9	327.7	0.64	0.74
	Ed4	272.5	343.4	0.47	0.59	252.1	310.1	0.58	0.70

Based on this sensitivity study (Table 3) along with the results of Tables 1 and 2, we have reached the following conclusions. For a given surface albedo, the positive biases (~8 W m^{-2}) in SW$^{\downarrow}_{sfc}$ flux using CM cloud retrievals and in SW$^{\uparrow}_{TOA}$ flux using ARM cloud retrievals are mainly attributed to the negative bias of −4.1% in CM τ retrievals. For given cloud properties, the flux differences between the RTM calculations and ARM PSP and CERES observations primarily result from the representativeness of the domain surface albedo. To reach a radiation closure study at both surface and TOA, the domain mean albedo must be used.

3.2.2 Radiation Closure Study Over Snow Surfaces

The comparisons of SW$^{\downarrow}_{sfc}$ flux and γ between the RTM calculations and the ARM surface PSP observations over snow surfaces are shown in Figures 12 and 13, and their statistical results are also listed in Table 2. Compared to the ARM PSP-observed SW$^{\downarrow}_{sfc}$ (279.0 W m^{-2}) for Terra cases, the RTM calculated SW$^{\downarrow}_{sfc}$ fluxes with input of ARM, Ed4, and Ed2 cloud retrievals are 273.0, 264.4, and 274.4 W m^{-2}, respectively. For Aqua cases, the RTM-calculated SW$^{\downarrow}_{sfc}$ fluxes using ARM, Ed4, and Ed2 cloud retrievals have positive biases of 3.0, 27.7, and 6.8 W m^{-2}, respectively, compared to the

ARM PSP observed $SW^{\downarrow}_{sfc}$ (278.0 W m^{-2}). The mean RTM-calculated $SW^{\downarrow}_{sfc}$ fluxes using ARM cloud retrievals agree with the ARM PSP observations within −1.5 W m^{-2} and have nearly identical γ values with the highest correlations ($R^2 = 0.81$ and 0.86) for Terra and Aqua. The RTM calculated $SW^{\downarrow}_{sfc}$ fluxes using Ed4/Ed2 cloud retrievals from both Terra and Aqua, on average, are 3.8 W m^{-2} higher than the ARM PSP observations due to the compensating effect of negative biases in Terra and positive biases in Aqua. Using Ed4 cloud retrievals only, the $SW^{\downarrow}_{sfc}$ flux differences are −4.6 W m^{-2} and 6.8 W m^{-2} for Terra and Aqua, almost the same as those using ARM cloud retrievals.

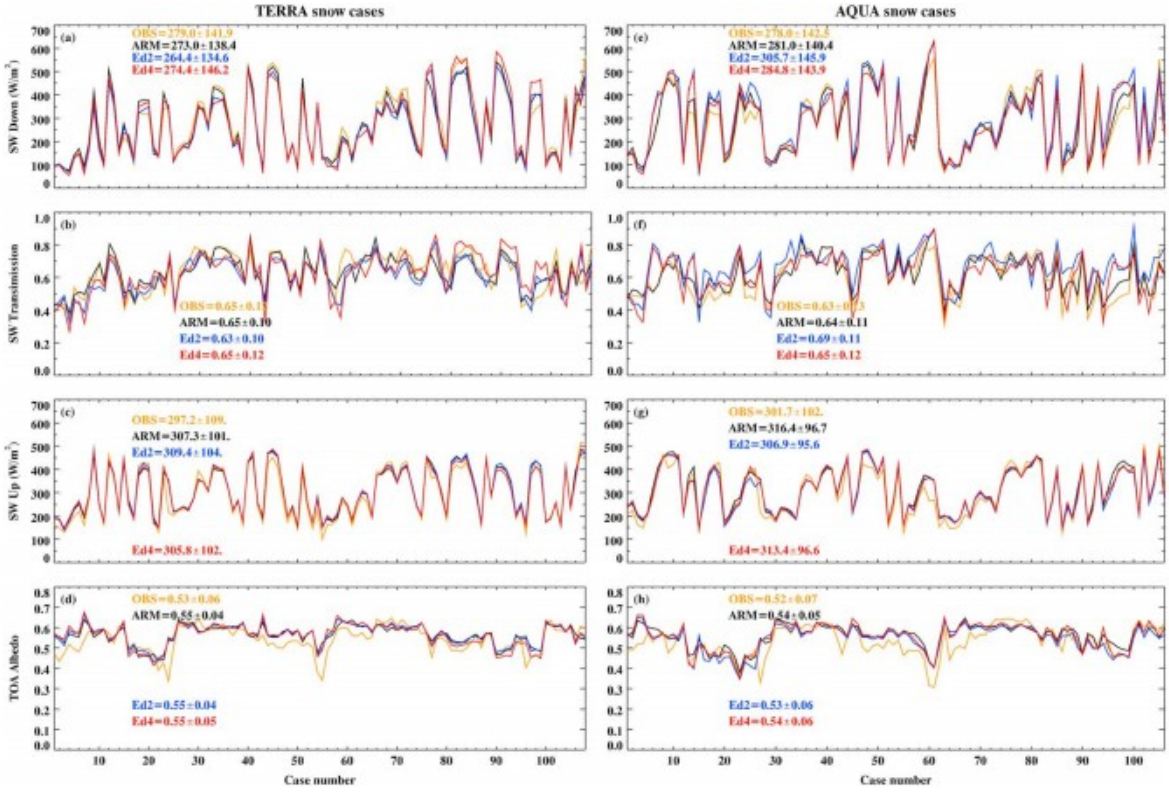

Figure 12. Same as Figure 10 except for snow cases.

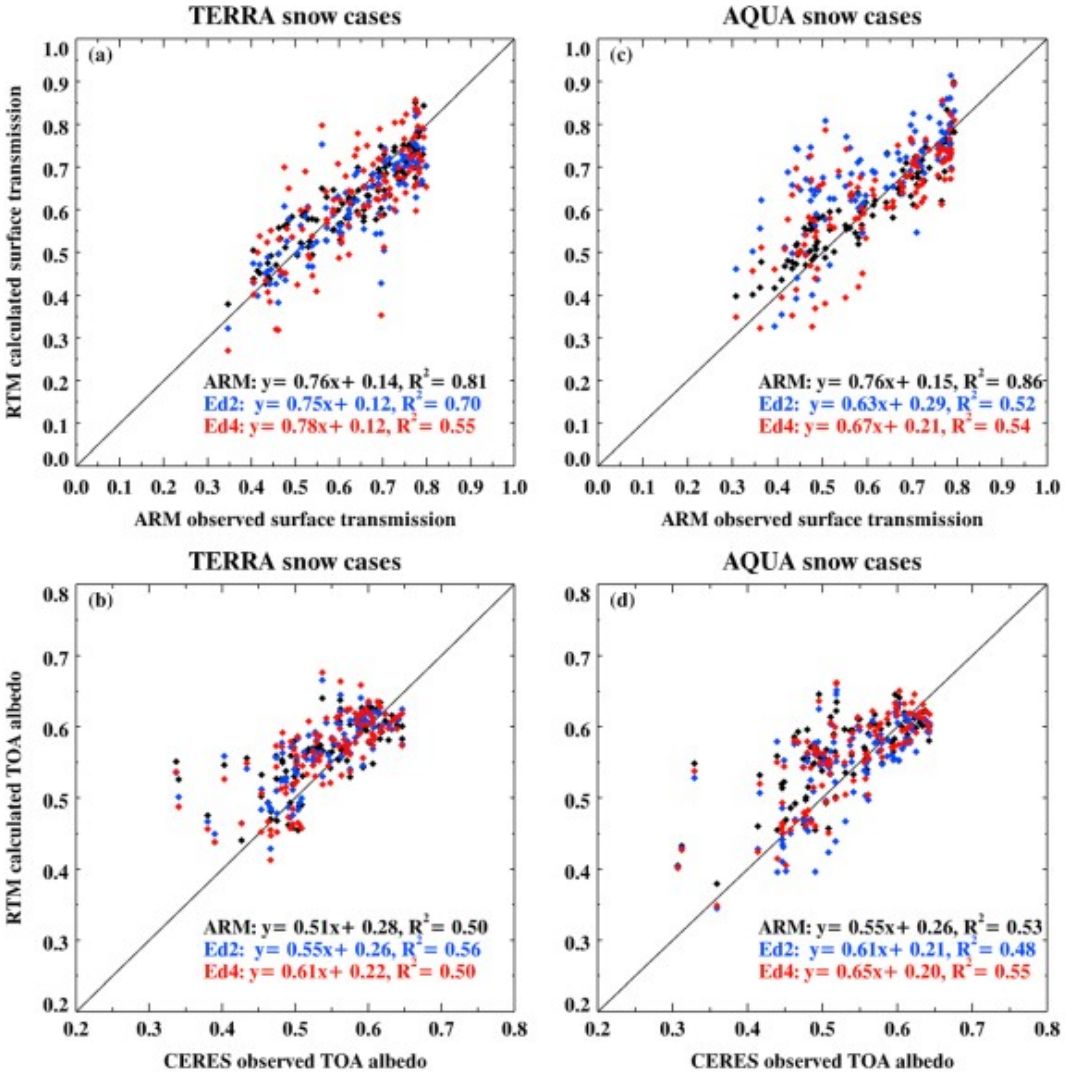

Figure 13. Same as Figure 11 except for snow cases.

The differences in $SW^{\uparrow}_{TOA}$ flux between the CERES observations and the RTM calculations using ARM and Ed4/Ed2 cloud retrievals over snow surfaces are close to, even slightly better, than the differences for snow-free cases. On average, the calculated $SW^{\uparrow}_{TOA}$ fluxes using ARM cloud retrievals are 12.4 W m^{-2} higher than CERES Terra and Aqua observations and 9.4 W m^{-2} higher using Ed4/Ed2 cloud retrievals. As a result, the calculated R_{TOA} values using three cloud retrievals are 0.02 higher than the CERES observation (0.53) with correlations of $R^2 = 0.50$–0.56 for Terra (Figure 13b), and 0.01–0.02 higher than the CERES observation (0.52) with correlations of $R^2 = 0.48$–0.55 for Aqua (Figure 13d).

A similar study was performed to investigate the flux differences between the RTM calculations and observations for snow cases, and the averages are listed in the bottom half of Table 3. The lower limit ($0.46 \times R_{sfc}$) and upper

limit (ARM PSP-measured R_{sfc}) of surface albedo are used as the domain albedo as discussed in section 2.4. The RTM calculations using these two limits represent the two extreme conditions, and they are either too high or too low compared to the ARM and CERES flux observations. The large positive biases in the RTM calculations using ARM PSP-measured R_{sfc} in Table 3 and much better agreements using the domain mean albedo in Table 2 demonstrate that the domain mean albedo is required in order to reach the radiation closure at both surface and TOA.

If we use the ARM PSP-measured R_{sfc} in ARM cloud retrievals and the RTM calculations, the averaged r_e and τ values would be 8.4 μm and 9.54 μm, and the RTM-calculated $SW^{\uparrow}_{TOA}$ and $SW^{\downarrow}_{sfc}$ fluxes would be 342.8 $W\,m^{-2}$ and 280.3 $W\,m^{-2}$ from the 108 Terra snow cases. Compared these values with those in Tables 1-3, it is understandable to have an excellent agreement in $SW^{\downarrow}_{sfc}$ flux due to the compensating effect of higher τ and surface albedo as discussed in the Appendix of *Dong and Mace* [2003]; however, the RTM-calculated $SW^{\uparrow}_{TOA}$ flux, on average, is 45.6 $W\,m^{-2}$ higher than the CERES observation.

3.2.3 Sensitivities of γ and R_{TOA} to *SZA* and R_{sfc}

To investigate how γ and R_{TOA} change with SZA and R_{sfc}, we plot Figures 14 and 15. Figures 14a and 14b show the dependence of γ and R_{TOA} on SZA from all Terra and Aqua snow-free cases, where the observed γ decreases from 0.6 to 0.4 and R_{TOA} increases from 0.36 to 0.46 when SZA is increased from 48° to 78°. This is understandable because at larger SZAs, more solar photons will be reflected back to space and fewer can penetrate through the cloud to reach the ground. Similar to the results in Figure 8, the calculated γ values using ARM cloud retrievals agree best with the ARM surface PSP observations, whereas the differences between the ARM PSP observations and the RTM calculations using Ed4/Ed2 cloud retrievals are also less than 0.05 for each bin. The R_{TOA} differences between CERES observations and RTM calculations are similar to their γ counterparts for each bin with the largest difference using ARM cloud retrievals but still less than 0.05. Figures 14c and 14d show the dependence of γ and R_{TOA} on SZA from all Terra and Aqua snow cases where a few significant differences exist compared to their snow-free counterparts. First of all, both γ and R_{TOA} values for snow cases are much larger than their snow-free counterparts due to the multiple reflections of solar radiation between the cloud layer and highly reflective surfaces. Second, both γ and R_{TOA} values increase from SZA = 48° to 66°, then decrease to 78°. Figure 14 demonstrates that the dependences of γ and R_{TOA} on SZA are significantly different for snow-free and snow-covered surfaces.

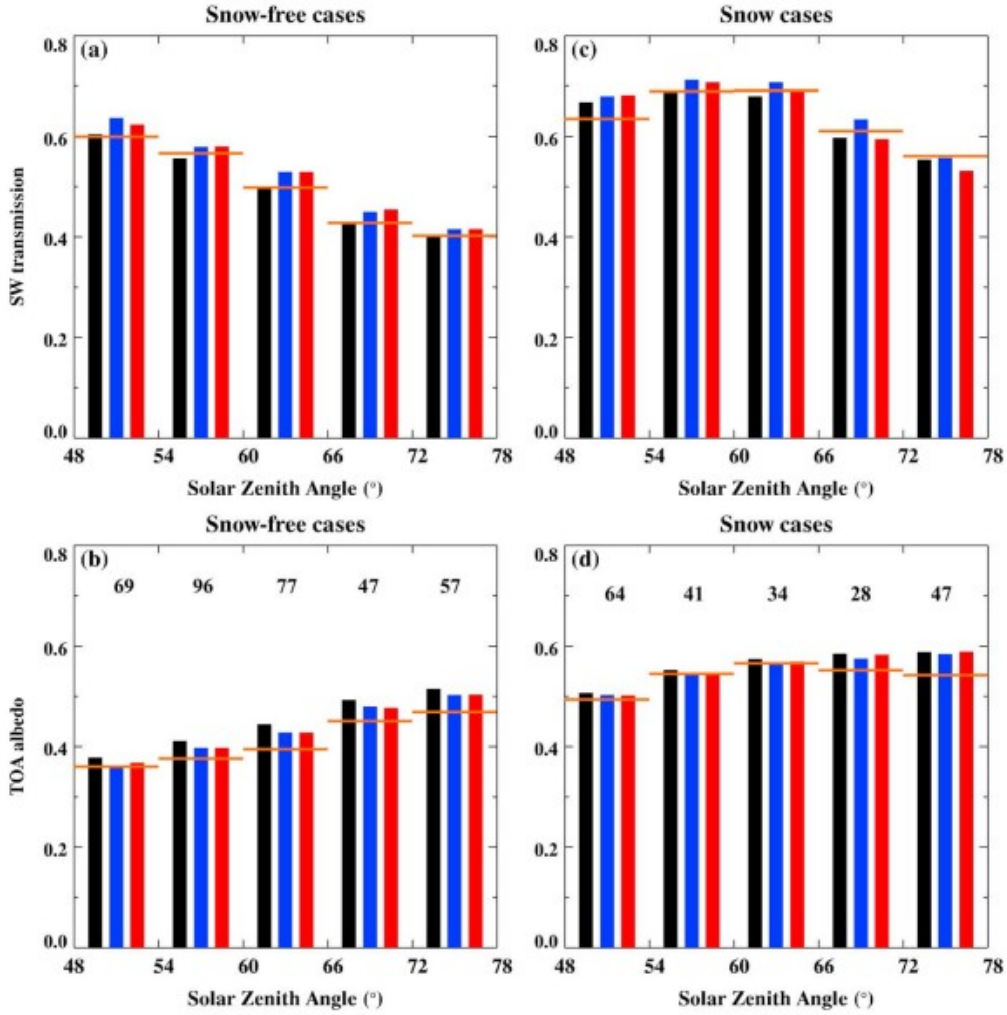

Figure 14. Sensivities of SW transmission γ at the surface and TOA albedo R_{TOA} to solar zenith angles (SZA) from both Terra and Aqua (left column) snow-free and (right column) snow cases. The brown lines represent the ARM PSP observed SW transmission γ at the surface and CERES observed TOA albedo R_{TOA} at each bin, and the color bars represent the RTM calculated γ and R_{TOA} using ARM (black), Ed4 (red), and Ed2 (blue) cloud retrievals as input. The numbers of samples in each bin are shown in Figures 14b and 14d.

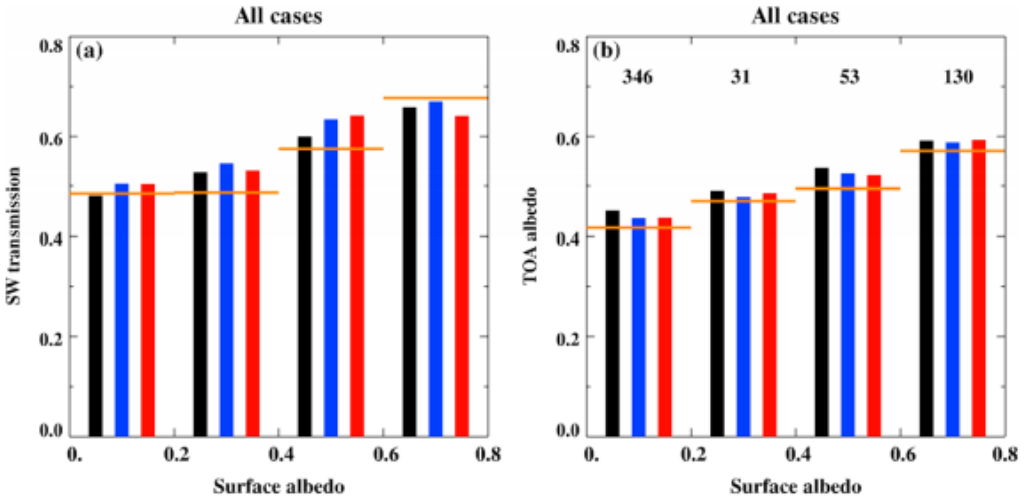

Figure 15. Same as Figure 14 except for the sensitivities of γ and R_{TOA} to the adjusted surface albedo from all Terra and Aqua snow-free and snow cases. The number of samples in each bin is shown in Figure 15b.

To demonstrate the impact of R_{sfc} on cloud albedo and γ, *Dong and Mace* [2003, Figure A1] used a two-stream discrete-ordinate method [*Liou*, 1974] and found both cloud albedo and γ rise with increasing R_{sfc}, and τ becomes less important with increasing R_{sfc}. When R_{sfc} is high, the multiple reflections of solar radiation between the cloud layer and highly reflective surfaces can contribute significantly to both cloud albedo (therefore R_{TOA}) and γ. The observed and calculated γ and R_{TOA} values in Figure 15 generally follow the trends of theoretical calculations in Figure A1 of *Dong and Mace* [2003]; i.e., they both increase with increasing R_{sfc}. The γ values increase from 0.47 to 0.68, and the R_{TOA} values rise from 0.42 to 0.57 when R_{sfc} is increased from 0.0 to 0.8. The differences between the RTM calculations and CERES observations are generally less than 0.07 and do not increase with increasing R_{sfc}.

4 Summary and Conclusions

The CERES Ed4 and Ed2 retrieved single-layered overcast cloud microphysical properties have been compared with the ground-based cloud retrievals at the ARM NSA site from March 2000 to December 2006. During the 7 year period, a total of 206 and 140 snow-free cases ($R_{sfc} \leq 0.3$), and 108 and 106 snow cases ($R_{sfc} > 0.3$), respectively, were selected from Terra and Aqua satellites overpass the ARM NSA site. These cloud microphysical properties, as well as ARM-measured cloud base and cloud top heights and R_{sfc}, were used as input for the NASA Langley modified Fu-Liou radiative transfer model (RTM) to calculate $SW^{\downarrow}_{sfc}$ flux and γ, and $SW^{\uparrow}_{toa}$ flux and R_{TOA}. These calculations were then compared with the collocated ARM surface and CERES TOA observations. Through an integrative analysis of the collocated satellite-surface data and the state-of-the-art RTM calculations, we briefly answer the three scientific questions posed in the beginning as follows:

1. The CERES Ed4 and Ed2 τ and *LWP* retrievals from both Terra and Aqua are almost identical and have excellent agreement with ARM retrievals under snow-free conditions. For r_e comparisons, the differences between Ed4 and Ed2, Terra and Aqua, are almost indistinguishable, but their mean values are ~2 μm greater than the ARM averages. The r_e, τ, and *LWP* comparisons between CERES Ed4/Ed2 and ARM over snow surfaces also agree well each other and are close to their snow-free counterparts with a few exceptions. Both ARM and CERES Ed4/Ed2 retrieved r_e, τ, and *LWP* values over snow surfaces are slightly smaller than their corresponding snow-free counterparts, and CERES Ed2 retrieved τ and *LWP* for Aqua cases over snow surfaces are much lower than ARM and CERES Ed4 retrievals. The Aqua Ed4 retrievals of τ and *LWP* are a significant improvement over the Ed2 results.
2. There is excellent agreement in both $SW^{\downarrow}_{sfc}$ flux and transmission measured at the surface with the Fu-Liou RTM calculations using ARM cloud retrievals as input, indicating a consistency check to the ARM cloud property retrievals where a δ2-stream radiative transfer model was employed. Based on the sensitivity study in Table 3 along with the results of Tables 1 and 2, we make the following conclusions. For a given surface albedo, the positive biases (~8 $W\,m^{-2}$) in $SW^{\downarrow}_{sfc}$ flux using CM cloud retrievals and in $SW^{\uparrow}_{TOA}$ flux using ARM cloud retrievals are mainly attributed to the negative bias of −4.1% in CM τ retrievals. For the given cloud properties, the flux differences between the RTM calculations and ARM PSP and CERES observations primarily result from the representativeness of the domain surface albedo. To reach a radiation closure study at both surface and TOA, the domain mean albedo must be used.
3. For snow cases, the mean RTM-calculated $SW^{\downarrow}_{sfc}$ fluxes using ARM and Ed4 cloud retrievals agree with the ARM PSP observations within 2 $W\,m^{-2}$ and have nearly identical γ values, whereas the differences using Aqua Ed2 cloud retrievals are relatively large due to their optical depth retrievals. The differences in $SW^{\uparrow}_{TOA}$ flux between the CERES observations and the RTM calculations using ARM and Ed4/Ed2 cloud retrievals over snow surfaces are close to, even slightly better, than the differences for snow-free cases. On average, the calculated $SW^{\uparrow}_{TOA}$ fluxes using ARM and Ed4/Ed2 cloud retrievals are 12.4 and 9.4 $W\,m^{-2}$, respectively, higher than the CERES observations. As a result, all calculated R_{TOA} values agree with the CERES observations to within 0.01–0.02.
4. Sensitivity studies showed that the ARM *LWPs* do not vary monotonically with SZA, whereas the CERES *LWPs* increase with SZA, particularly for the last bin. Both CERES and ARM r_e retrievals are less dependent on SZA, and their differences are within ~2 μm except for the last bin. All retrieved optical depths increase with increasing SZA

over snow-free surfaces, whereas over snow, both CERES and ARM retrieved τ values decrease with SZA, and then increase in last two bins, similar to their *LWP* comparisons. Both CERES and ARM cloud retrievals have similar dependencies on R_{sfc} and agree very well each other except for a couple of bins. The SW transmission γ decreases while R_{TOA} increases with increasing SZA for snow-free surfaces. For snow cases, however, there are a few significant differences due to the multiple reflections of solar radiation between the cloud layer and highly reflective surfaces.

Given the excellent agreements in cloud property retrievals, $SW^{\downarrow}_{sfc}$ flux and transmission γ at the surface, and $SW^{\uparrow}_{TOA}$ flux and R_{TOA} between the ARM and CERES observations and the Fu-Liou RTM calculations using ARM and CERES Ed4/Ed2 cloud retrievals as input, we conclude that a radiation closure study of Arctic stratus cloud microphysical properties is reached. In order to make apples-to-apples comparisons between ARM and CM cloud retrievals and reach a radiation closure study at both surface and TOA, the ARM PSP-measured surface albedos were adjusted to account for the water and land components of the domain. The domain surface albedos were estimated to be 63.6% and 80% of the ARM PSP-measured surface albedos and were used for the snow-free and snow cases, respectively, in this study. The results reported here represent only a small subset of Arctic cloud conditions, single-layer and overcast liquid water clouds, over a single site. Additional comparisons for a greater variety of cloud conditions and over other polar backgrounds are needed to fully evaluate the CERES retrievals of cloud properties and surface fluxes.

Acknowledgments

The ground-based measurements were obtained from the Atmospheric Radiation Measurement (ARM) Program sponsored by the U.S. Department of Energy (DOE) Office of Energy Research, Office of Health and Environmental Research, Environmental Sciences Division. The data can be downloaded from http://www.archive.arm.gov/. The satellite data were obtained from the NASA CERES cloud working group at NASA Langley Research Center. Special thanks to Seiji Kato for the useful discussion about NASA Langley Modified Fu-Liou radiative transfer model. This research was supported by the NASA CERES project under grant NNX14AP84G at the University of North Dakota and by the DOE ARM Program under contract DE-SC0013896 at NASA Langley. Dates and times corresponding to the sample numbers used in several figures are available from the lead author on request (dong@aero.und.edu).

References

Ackerman, T. P., and G. M. Stokes (2003), The Atmospheric Radiation Measurement Program, *Phys. Today*, 56, 38– 44.

Chen, Y., S. Sun-Mack, P. Minnis, and R. F. Arduini (2006), Clear-sky narrowband albedo variations derived from VIRS and MODIS data. *Proc. AMS 12th Conf. Atmos. Radiation*, Madison, WI, July 10-14, CD-ROM, 5.6.

Chen, Y., P. Minnis, S. Sun-Mack, R. F. Arduini, and Q. Z. Trepte (2010), Clear-sky and surface narrowband albedo datasets derived from MODIS data, *Proc. AMS 13th Conf. Atmos. Rad. and Cloud Phys.*, Portland, OR, June 27–July 2, JP1.2.

Clothiaux, E. E., T. P. Ackerman, G. G. Mace, K. P. Moran, R. T. Marchand, M. A. Miller, and B. E. Martner (2000), Objective determination of cloud heights and radar reflectivities using a combination of active remote sensors at the Atmospheric Radiation Measurement Program Cloud and Radiation Test Bed (ARM CART) sites, *J. Appl. Meteorol.*, 39, 645– 665.

Curry, J. A., W. B. Rossow, D. Randall, and J. L. Schramm (1996), Overview of Arctic cloud and radiation characteristics, *J. Clim.*, 9, 1731– 1764.

Curry, J. A., et al. (2000), FIRE Arctic clouds experiment, *Bull. Am. Meteorol. Soc.*, 81, 5– 29.

Dong, X., and G. G. Mace (2003), Arctic stratus cloud properties and radiative forcing derived from ground-based data collected at Barrow, Alaska, *J. Clim.*, 16, 445– 461.

Dong, X., T. P. Ackerman, E. E. Clothiaux, P. Pilewskie, and Y. Han (1997), Microphysical and radiative properties of stratiform clouds deduced from ground-based measurements, *J. Geophys. Res.*, 102, 23,829– 23,843, doi:10.1029/97JD02119.

Dong, X., T. P. Ackerman, and E. E. Clothiaux (1998), Parameterizations of microphysical and shortwave radiative properties of boundary layer stratus from ground-based measurements, *J. Geophys. Res.*, 102, 31,681– 31,393, doi:10.1029/1998JD200047.

Dong, X., P. Minnis, T. P. Ackerman, E. E. Clothiaux, G. G. Mace, C. N. Long, and J. C. Liljegren (2000), A 25-month database of stratus cloud properties generated from ground-based measurements at the Atmospheric Radiation Measurement Southern Great Plains Site, *J. Geophys. Res.*, 105, 4529– 4537, doi:10.1029/1999JD901159.

Dong, X., G. G. Mace, P. Minnis, and D. F. Young (2001), Arctic stratus cloud properties and their effect on the surface radiation budget: Selected cases from FIRE ACE, *J. Geophys. Res.*, 106(15), 15,297– 15,312, doi:10.1029/2000JD900404.

Dong, X., P. Minnis, G. G. Mace, W. L. Smith Jr., M. Poellot, R. Marchand, and A. Rapp (2002), Comparison of stratus cloud properties deduced from surface, GOES, and aircraft data during the March 2000 ARM Cloud IOP, *J. Atmos. Sci.*, 59, 3265– 3284.

Dong, X., P. Minnis, and B. Xi (2005), A climatology of midlatitude continental clouds from ARM SGP site. Part I: Low-level cloud macrophysical, microphysical and radiative properties, *J. Clim.*, 18, 1391– 1410.

Dong, X., P. Minnis, B. Xi, S. Sun-Mack, and Y. Chen (2008), Validation of CERES-MODIS stratus cloud properties using ground-based measurements at the DOE ARM SGP site, *J. Geophys. Res.*, 113, D03204, doi:10.1029/2007JD008438.

Dong, X., B. Xi, K. Crosby, C. N. Long, R. Stone, and M. Shupe (2010), A 10-yr climatology of Arctic cloud fraction and radiative forcing at Barrow, Alaska, *J. Geophys. Res.*, 115, D12124, doi:10.1029/2009JD013489.

Intrieri, J. M., M. D. Shupe, T. Uttal, and B. J. McCarty (2002), An annual cycle of Arctic cloud characteristics observed by radar and lidar at SHEBA, *J. Geophys. Res.*, 107(C10), 8030, doi:10.1029/2000JC000423.

Kato, S., F. G. Rose, and T. P. Charlock (2005), Computation of domain averaged irradiance using satellite-derived cloud properties, *J. Atmos. Oceanic Technol.*, 22, 146– 164.

Liljegren, J. C., E. E. Clothiaux, G. G. Mace, S. Kato, and X. Dong (2001), A new retrieval for cloud liquid water path using a ground-based microwave radiometer and measurements of cloud temperature, *J. Geophys. Res.*, 106, 14,485– 14,500, doi:10.1029/2000JD900817.

Liou, K. N. (1974), Analytic two-stream and four-stream solutions for radiative transfer, *J. Atmos. Sci.*, 31, 1473– 1475.

Loeb, N. G., S. Kato, K. Loukachine, and N. Manalo-Smith (2005), Angular distribution models for top-of-atmosphere radiative flux estimation from the Clouds and the Earth's Radiant Energy System instrument on the Terra satellite. Part I: Methodology, *J. Atmos. Oceanic Technol.*, 22, 338– 351.

Loeb, N. G., S. Kato, K. Loukachine, N. Manalo-Smith, and D. R. Doelling (2007), Angular distribution models for top-of-atmosphere radiative flux estimation from the Clouds and the Earth's Radiant Energy System instrument on the Terra satellite. Part II: Validation, *J. Atmos. Oceanic Technol.*, 24, 564– 584.

Loeb, N. G., B. A. Wielicki, D. R. Doelling, G. L. Smith, D. F. Keyes, S. Kato, N. Manalo-Smith, and T. Wong (2009), Toward optimal closure of the Earth's top-of-atmosphere radiation budget, *J. Clim.*, 22(3), 748– 766.

Long, C. N., and T. P. Ackerman (2000), Identification of clear skies from broadband pyranometer measurements and calculation of downwelling shortwave cloud effects, *J. Geophys. Res.*, 105, 15,609– 15,626, doi:10.1029/2000JD900077.

Long, C. N., and Y. Shi (2008), An automated quality assessment and control algorithm for surface radiation measurements, *Open Atmos. Sci. J.*, 2, 23– 37, doi:10.2174/1874282300802010023.

Miles, N. L., J. Verlinde, and E. E. Clothiaux (2000), Cloud-droplet size distributions in low-level stratiform clouds, *J. Atmos. Sci.*, 57, 295– 311.

Minnis, P., et al. (2008), Cloud detection in non-polar regions for CERES using TRMM VIRS and Terra and Aqua MODIS data, *IEEE Trans. Geosci. Remote Sens.*, 46, 3857– 3884.

Minnis, P., et al. (2010a), CERES Edition 3 cloud retrievals. *AMS 13th Conf. Atmos. Rad.*, Portland, OR, June 27 – July 2, 5.4.

Minnis, P., et al. (2010b), CERES Ed3 cloud algorithm update, *13th CERES-II Sci. Team Mtg.*, Newport News, VA, Apr. 27–29. [Available at http://ceres.larc.nasa.gov/documents/STM/2011-04/3_Minnis_Clouds_0411.pdf.]

Minnis, P., et al. (2011a), CERES Edition-2 cloud property retrievals using TRMM VIRS and Terra and Aqua MODIS data, Part I: Algorithms, *IEEE Trans. Geosci. Remote Sens.*, 49, 4374– 4399.

Minnis, P., et al. (2011b), CERES Edition-2 cloud property retrievals using TRMM VIRS and Terra and Aqua MODIS data, Part II: Examples of average results and comparisons with other data, *IEEE Trans. Geosci. Remote Sens.*, 49, 4401– 4430.

Moran, K. P., B. E. Martner, M. J. Post, R. A. Kropfli, D. C. Welsh, and K. B. Widener (1998), An unattended cloud-profiling radar for use in climate research, *Bull. Am. Meteorol. Soc.*, 79(3), 443– 455.

Nakajima, T., and M. D. King (1990), Determination of the optical thickness and effective particle radius of clouds from reflected solar radiation measurements. Part I: Theory, *J. Atmos. Sci.*, 47, 1878– 1893.

NASA (2014), Single Scanner Footprint TOA/Surface Fluxes and Clouds (SSF), CERES Data Products Catalog, DPC-SSF-Ed4 R5V1, 20 June, 17 pp. [Available at http://ceres.larc.nasa.gov/documents/DPC/DPC_current/pdfs/DPC_SSF-Ed4_R5V1.pdf.]

NASA (2016), CERES Terra & Aqua Edition4A SSF Cloud Properties - Accuracy and Validation, CERES SSF_Terra-Aqua_Edition4A Data Quality Summary, 17 March, 42 pp. [Available at https://eosweb.larc.nasa.gov/sites/default/files/project/ceres/quality_summaries/ssf_cloud_prop_terra-aqua_Ed4A.pdf.]

Qiu, S., X. Dong, B. Xi, X. Dong, and J.-L. F. Li (2015), Characterizing Arctic mixed-phase cloud structure and its relationship with humidity and temperature inversion using ARM NSA observations, *J. Geophys. Res. Atmos.*, 120, 7737– 7746, doi:10.1002/2014JD023022.

Rose, F., T. Charlock, Q. Fu, S. Kato, D. Rutan, and Z. Jin (2006), CERES proto-edition 3 radiative transfer: Tests and radiative closure over surface validation sites, paper presented at 12th Conference on Atmospheric Radiation (AMS), 10–14 July 2006, Madison, Wis.

Rutan, D., F. Rose, M. Roman, N. Manalo-Smith, C. Schaaf, and T. Charlock (2009), Development and assessment of broadband surface albedo from Clouds and the Earth's Radiant Energy System Clouds and Radiation Swath data product, *J. Geophys. Res.*, 114, D08125, doi:10.1029/2008JD010669.

Spangenberg, D. A., Q. Trepte, P. Minnis, and T. Uttal (2004), Daytime cloud property retrievals over the Arctic from multispectral MODIS data, *Proc. 13th AMS Conf. Satellite Oceanogr. And Meteorol*, Norfolk, VA, Sept. 20–24, CD-ROM, P7.11.

Su, W., J. Corbett, Z. Eitzen, and L. Liang (2015a), Next-generation angular distribution models for top-of-atmosphere radiative flux calculation from CERES instruments: Methodology, *Atmos. Meas. Tech.*, 8(2), 611– 632.

Su, W., J. Corbett, Z. Eitzen, and L. Liang (2015b), Next-generation angular distribution models for top-of-atmosphere radiative flux calculation from CERES instruments: Validation, *Atmos. Meas. Tech.*, 8(8), 3297– 3313.

Trepte, Q., P. Minnis, and R. F. Arduini (2002), Daytime and nighttime polar cloud and snow identification using MODIS data. *Proc. SPIE 3rd Intl. Asia-Pacific Environ. Remote Sensing Symp.*, *2002: Remote Sens. Of Atmosphere, Ocean, Environment, an Space,* Hangzhou, China, October 23–27, vol. 4891, 449–459.

Uttal, T., et al. (2002), Surface heat budget of the Arctic Ocean, *Bull. Am. Meteorol. Soc.*, 83(2), 255– 275.

Verlinde, J., et al. (2007), The mixed-phase Arctic cloud experiment, *Bull. Am. Meteorol. Soc.*, 88(2), 205– 221.

Wielicki, B. A., et al. (1998), Clouds and the Earth's Radiant Energy System (CERES): Algorithm overview, *Trans. Geosci. Remote Sens.*, 36(4), 1127– 1141.

Xi, B., X. Dong, P. Minnis, and S. Sun-Mack (2014), Comparison of marine boundary layer cloud properties From CERES-MODIS Edition 4 and DOE ARM AMF measurements at the Azores, *J. Geophys. Res. Atmos.*, 119, 9509– 9529, doi:10.1002/2014JD021813.

Younkin, K., and C. N. Long (2003), Improved correction of IR loss in diffuse shortwave measurements: AM ARM value-added product, DOE ARM Tech. Rep. TR-09, Richland, Wash. [Available at http://www.arm.gov/publications/tech_reports/arm-tr-009.pdf.]